Alignments, additivity, and signature inversion in odd-odd ^{170}Ta: A comprehensive high-spin study

A. Aguilar,[1,*] D. J. Hartley,[2] M. A. Riley,[1] C. Teal,[1,†] M. P. Carpenter,[3] P. Chowdhury,[4] M. Danchev,[5,‡] M. K. Djongolov,[5,§] G. B. Hagemann,[6] A. A. Hecht,[3,‖] R. V. F. Janssens,[3] F. G. Kondev,[7] T. Lauritsen,[3] W. C. Ma,[8] W. H. Mohr,[2] E. F. Moore,[3] S. W. Ødegärd,[9] L. L. Riedinger,[5] G. Sletten,[6] S. K. Tandel,[4] J. R. Vanhoy,[2] X. Wang,[1] and S. Zhu[3]

[1]*Department of Physics, Florida State University, Tallahassee, Florida 32306, USA*
[2]*Department of Physics, U.S. Naval Academy, Annapolis, Maryland 21402, USA*
[3]*Physics Division, Argonne National Laboratory, Argonne, Illinois 60439, USA*
[4]*Department of Physics, University of Massachusetts Lowell, Lowell, Massachusetts 01854, USA*
[5]*Department of Physics and Astronomy, University of Tennessee, Knoxville, Tennessee 37996, USA*
[6]*The Niels Bohr Institute, Blegdamsvej 17, DK-2100 Copenhagen, Denmark*
[7]*Nuclear Engineering Division, Argonne National Laboratory, Argonne, Illinois 60439, USA*
[8]*Department of Physics, Mississippi State University, Mississippi State, Mississippi 39762, USA*
[9]*Department of Physics, University of Oslo, PB 1048 Blindern, N-0316 Oslo, Norway*

(Received 10 March 2010; published 21 June 2010)

High-spin states ($I \lesssim 50\hbar$) of the odd-odd nucleus ^{170}Ta have been investigated with the ^{124}Sn(^{51}V,5n) reaction. The resolving power of Gammasphere has allowed for the observation of eleven rotational bands (eight of which are new) and over 430 transitions (∼350 of which are new) in this nucleus. Many interband transitions have been observed such that the relative spins and excitation energies of the 11 bands have been established. This is an unusual circumstance in an odd-odd study. Configurations have been assigned to most of these bands based upon features such as alignment properties, band crossings, $B(M1)/B(E2)$ ratios, and the additivity of Routhians. A systematic study of the frequency at which normal signature ordering occurs in the $\pi h_{9/2}\nu i_{13/2}$ band has been performed and it is found that its trend is opposite to that observed in the $\pi h_{11/2}\nu i_{13/2}$ bands. A possible interpretation of these trends is discussed based on a proton-neutron interaction.

DOI: 10.1103/PhysRevC.81.064317 PACS number(s): 21.10.Re, 23.20.Lv, 27.70.+q

I. INTRODUCTION

The complexity of odd-odd nuclei makes these isotopes particularly challenging to study. However, they often provide a wealth of nuclear structure phenomena such as twin bands [1], chiral bands [2], and signature inversion [3]. The nucleus ^{170}Ta was last investigated by Zhang *et al.* [4] and three rotational bands were observed up to spins near $23\hbar$. As with most odd-odd nuclei, the high-spin states could not be connected with the low-spin levels known from β or electron capture (EC) decay [5]. Thus, the absolute spins could not be determined. In addition, the relative spins were not established because no interband transitions were identified; another common feature in many odd-odd nuclei. In the present study, over 350 new transitions and eight new bands were added to the ^{170}Ta level scheme. This includes many interband transitions such that the relative spins can be confirmed for the bands. Configurations have been assigned for eight of the eleven bands, based upon properties such as their rotational alignments, band crossings, $B(M1)/B(E2)$ ratios (when possible), and the additivity of Routhians.

As mentioned, signature inversion (where the expected favored signature lies higher in excitation energy than its partner) is a phenomenon well established in odd-odd nuclei. In particular, the effect has been widely seen in the $\pi h_{11/2}\nu i_{13/2}$ configuration and many systematic studies have been performed to investigate its origin (see Refs. [6,7]). Theoretical calculations have led to several possible explanations including the presence of triaxiality [3,8], Coriolis mixing of a large number of bands [9], and the influence of a proton-neutron (pn) interaction [10–12]. The signature inversion in the $\pi h_{9/2}\nu i_{13/2}$ bands has not been as well studied; however, in principle the same explanation for the inversion in the $\pi h_{11/2}\nu i_{13/2}$ bands should apply to the former. Trends in the reversion frequency (i.e., the frequency at which the expected favored signature becomes lower in energy than its partner) have been investigated for the $\pi h_{9/2}\nu i_{13/2}$ bands in the $A \approx 170$ region. These trends can be explained by relating the particle- or hole-like character of the valence particles with a pn interaction [10].

II. EXPERIMENTAL DETAILS

High-spin states in ^{170}Ta were populated in the ^{124}Sn(^{51}V,5n) fusion-evaporation reaction using a 228-MeV

*Present address: Department of Radiation Oncology, University of Pennsylvania, Philadelphia, Pennsylvania 19104, USA.
†Present address: Nuclear Regulatory Commission T427, 11555 Rockville Pike, Rockville, Maryland 20855. Disclaimer: The views presented in this paper represent those of the authors alone and are not necessarily those of the NRC.
‡Present address: Saint Kliment Ohridski University of Sophia, BG-1164 Sofia, Bulgaria.
§Present address: TRIUMF, 4004 Westbrook Mall, Vancouver, British Columbia, V6T 2A3, Canada.
‖Also at Department of Chemistry, University of Maryland, College Park, Maryland 20742, USA; present address: Department of Chemical and Nuclear Engineering, The University of New Mexico, Albuquerque, New Mexico, 87131, USA.

beam provided by the ATLAS facility at Argonne National Laboratory. The target was composed of two $\sim$500 μg/cm^2 self-supporting foils of ^{124}Sn. Gamma rays were detected with the Gammasphere spectrometer, which consisted of 100 Compton-suppressed Ge detectors [13]. A total of $\sim 2 \times 10^9$ events of fold four or higher were recorded over four days of beam time. The RADWARE suite of programs [14] was used to create γ-γ-γ cubes and γ-γ-γ-γ hypercubes to study the coincidence relationships to construct the intricate level scheme of this odd-odd nucleus. It is worth noting that this experiment has resulted in two other publications that focused on the 4n and 6n channels, respectively [15,16].

A Blue database [17] was used to determine the relative spins of states by an angular correlation analysis. Sixteen spectra (one for each ring of Gammasphere) were produced by double-gating on two known $E2$ transitions in each rotational sequence, and background subtraction was performed utilizing the method of Starosta *et al.* [18]. An angular correlation ratio for the coincident γ rays was deduced using $R_{\rm ang} = W(\theta_f, \phi)/W(\theta_{90^\circ}, \phi)$, where $W(\theta_f, \phi)$ is the intensity observed in the forward detectors ($\theta = 122^\circ, 130^\circ, 143^\circ, 148^\circ$, and 163°) and $W(\theta_{90^\circ}, \phi)$ is the intensity observed in the detectors near 90° ($\theta = 79^\circ, 81^\circ, 90^\circ, 99^\circ$, and 101°). This ratio was normalized such that known $E2$ transitions had a value of $R_{\rm ang} \approx 1.0$. Spins for the highest lying transitions were assigned by assuming a consistent rotational behavior when $R_{\rm ang}$ could not be measured.

III. LEVEL SCHEME

The ground state for ^{170}Ta was suggested to have quantum numbers $I^\pi = (3^+)$ by Leber *et al.* [19], based upon the electron capture decay of ^{170}Ta into ^{170}Hf. Meissner *et al.* [5] observed a few γ rays that could be associated with ^{170}Ta resulting from the electron capture decay of ^{170}W. However, none of these transitions have been observed in high-spin studies of ^{170}Ta [4,20], indicating that they are likely originating from the deexcitation of low-spin states.

In the most recent work on ^{170}Ta, Zhang *et al.* [4] observed three rotational sequences up to medium spin ($\sim 23\hbar$). These bands were confirmed, as well as extended, in the present study and are labeled as bands 1 and 2 in Fig. 1 and band 6 in Figs. 2 and 3. Owing to the complexity and richness of the ^{170}Ta level scheme it is displayed in three separate figures. It should be noted that interband transitions were identified for all the bands; thus, their relative excitation energies have now been established. The spin and parity assignments must be regarded as tentative for all states as it is unlikely that any of the transitions feeds the ground state. However, the relative spin assignments for most of the bands have been confirmed with the angular correlation ratios of the linking transitions. Table I lists the spin, parity, and excitation energy of the states, as well as the γ-ray energies, intensities, and angular correlation ratios observed for the transitions in ^{170}Ta.

A. Negative-parity bands

Band 1 in Fig. 1 was previously assigned as a negative-parity band based upon the proposed $\pi h_{11/2} \nu i_{13/2}$ configuration [4]. We are in agreement with this assignment (see Sec. IV A) and the associated negative parity. Zhang *et al.* [4] plotted the energy level systematics for the $\pi h_{11/2} \nu i_{13/2}$ structures to assign spins to the states, and we have adopted these assignments as well. A sample spectrum of this strongly coupled sequence is displayed in Fig. 4(a). Four transitions (89, 97, 123, and 228 keV) were added below the previously observed lowest level (10^-), and the band was extended from $I = 22\hbar$ up to spin $46\hbar$. The energies of these states, minus a rigid-rotor reference, have been plotted in Fig. 5(a), along with the other negative-parity bands in ^{170}Ta. As seen in this figure, the $\alpha = 1$ signature of band 1 generally comprises the yrast sequence of ^{170}Ta, except for a few states near $I = 20\hbar$, where band 2 is nominally lower in energy.

Previously, the structure labeled as band 2 in Fig. 1 was also assigned negative parity based upon the proposed $\pi h_{9/2} \nu i_{13/2}$ configuration [4]. This assignment is confirmed here through the observation of many interband transitions between bands 1 and 2, as displayed in the level scheme of Fig. 1. Respective angular correlation ratios of 1.10(3) and 0.82(4) for the 585- and 610-keV linking transitions are indicative of an $E2$ character and suggest that there is strong mixing between the 19^- states of bands 1 and 2. These ratios solidify the fact that bands 1 and 2 have the same (negative) parity and confirm the proposed spins of Zhang *et al.* [4]. Three transitions (86, 137, and 191 keV) were placed below the lowest level (8^-) previously observed, and a fourth (51 keV) is assumed based on coincidence relationships, but could not be observed owing to its low energy and its likely high electron conversion coefficient. Band 2 was extended from $I = 24\hbar$ to $43\hbar$, and spectra for the $\alpha = 0$ and 1 sequences are presented in Figs. 4(b) and 4(c), respectively. Inspection of Fig. 5(a) indicates that the $\alpha = 0$ signature lies very close in energy to band 1 below $20\hbar$ and that the $\alpha = 1$ signature is nearly degenerate with band 1 in the spin range of $17\hbar$–$33\hbar$. This near degeneracy accounts naturally for the presence of the interband transitions between the two bands over a large spin range, as seen in Fig. 1.

A new, decoupled structure that feeds band 2 at lower spins was observed and is labeled as band 3 in Fig. 1. Figure 6(a) displays not only the inband transitions but also the strong connecting γ rays feeding band 2. Angular correlation ratios for the 397-, 473-, and 536-keV lines were measured to be 0.51(4), 0.50(4), and 0.61(7), respectively. These values are consistent with $\Delta I = 1$ transitions and help assign the relative spins of band 3; however, the relative parity assignment is not as clear as these could be either of $E1$ or $M1$ character. Based on the proposed configuration assignment (see Sec. IV C), we have assigned negative parity to band 3. Although band 3 lies at high excitation energy with respect to the other observed bands at lower spins [see Fig. 5(a)], its energy is comparable with many of the positive-parity sequences above $I = 20\hbar$.

A weaker, decoupled sequence was observed feeding into band 3 near $I = 24\hbar$, and it is denoted as band 4 in Fig. 1. A spectrum of the band is given in Fig. 6(b). The linking transition was too weak to perform a reliable angular correlation analysis; therefore, a definitive spin assignment could not be proposed. If the assumption is made that the linking transition is of $E2$ character, the $I = 24\hbar$ states of

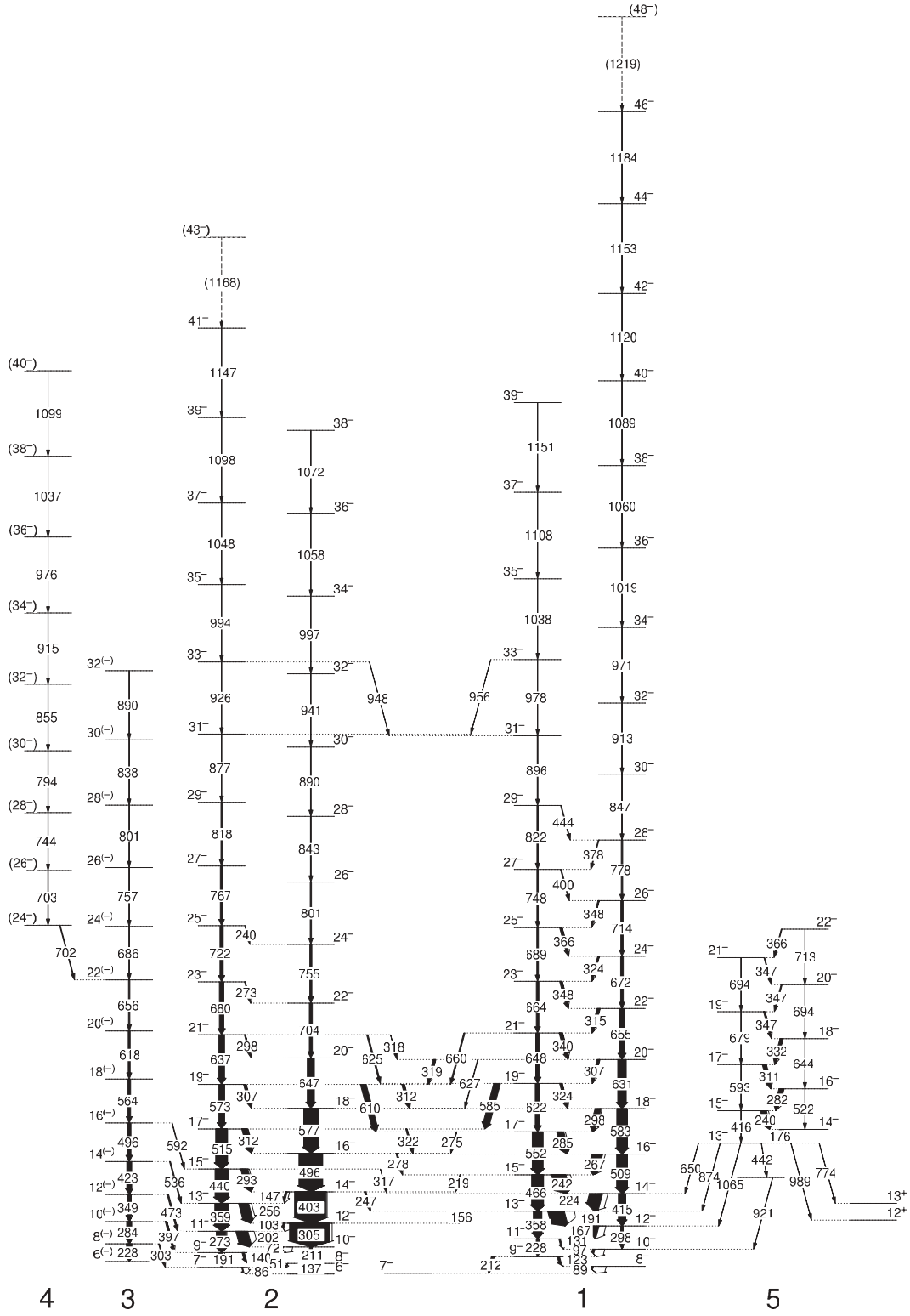

FIG. 1. Partial level scheme of ^{170}Ta displaying negative-parity sequences. Tentatively placed γ rays are denoted with a dashed line.

bands 3 and 4 would be nearly degenerate, as seen in Fig. 5(a), which provides a natural explanation for why band 4 feeds into band 3 at this spin. The spin assignment is based upon this reasoning, but it must be regarded as tentative. It should also be noted that band 4 approaches the yrast line rapidly at higher spins; this is the likely reason that this weaker structure is observed up to such high spins ($40\hbar$).

The sequence labeled band 5 in Fig. 1 is strongly -coupled and was important for determining the relative excitation energies of all the bands since it feeds both positive- and

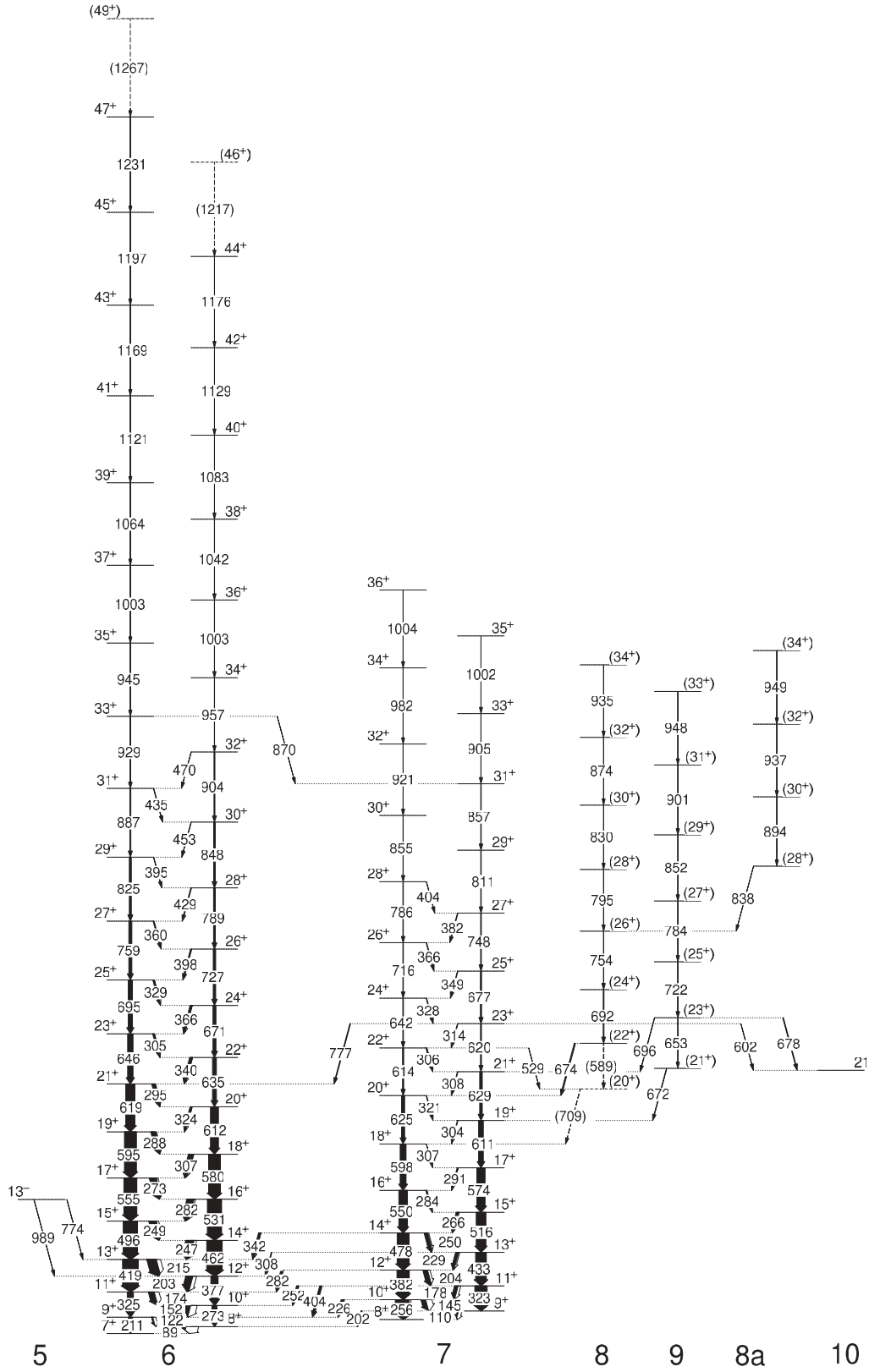

FIG. 2. Partial level scheme of ^{170}Ta displaying the positive-parity bands 6, 7, 8, 8a, and 9. Tentatively placed γ rays are denoted with a dashed line.

negative-parity structures. It comprises intense $\Delta I = 1$ transitions and rather weak $\Delta I = 2$ ones as seen in the spectrum of Fig. 6(c). The spins and parity of the band were determined analytically by the transitions feeding out of the bottom of the band to bands 1 and 6. The 14^-, 13^-, and 12^- levels in band 1 are fed by band 5. This implies that the spin of the lowest

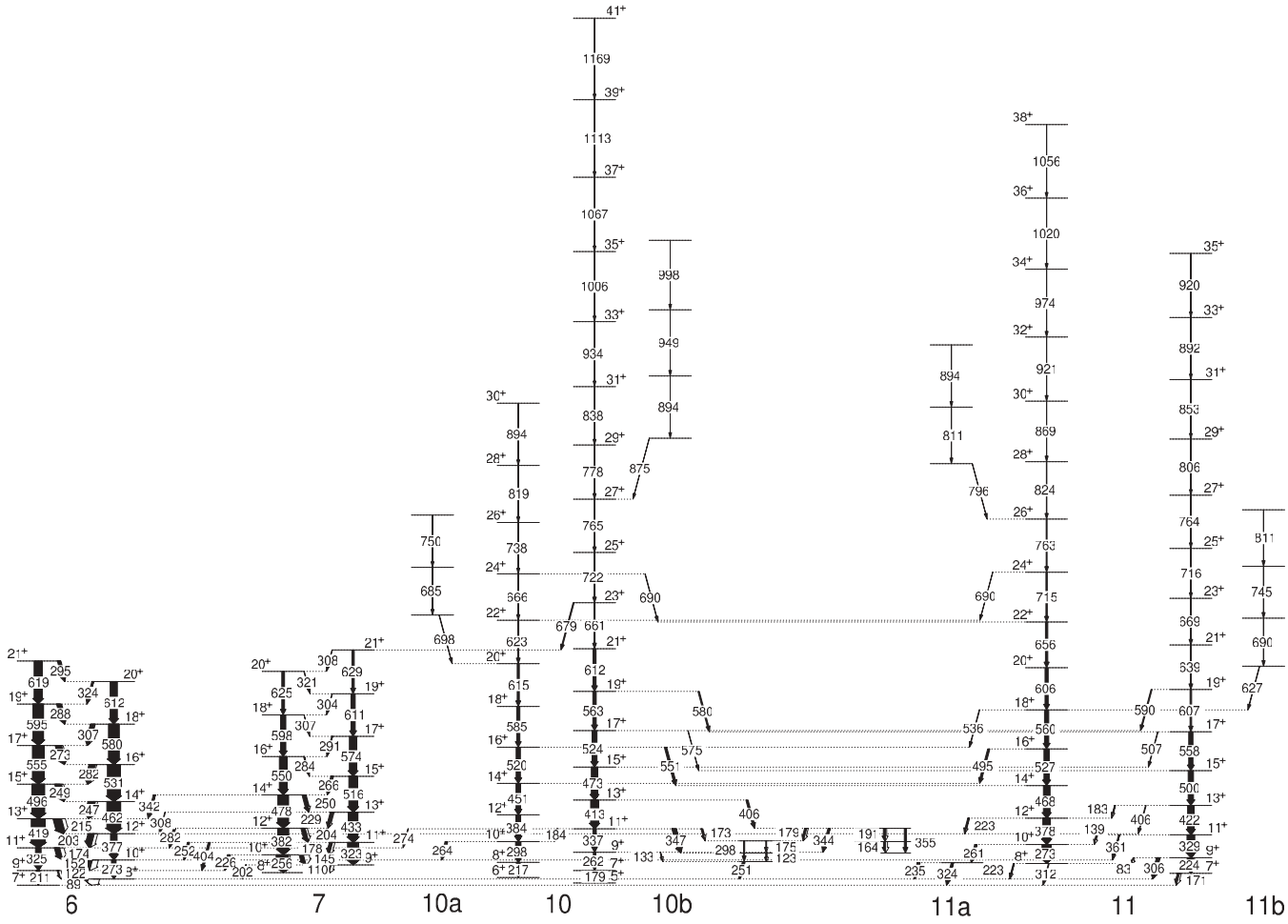

FIG. 3. Partial level scheme of ^{170}Ta displaying the positive-parity bands 10, 10a, 10b, 11, 11a, and 11b. Tentatively placed γ rays are denoted with a dashed line.

level in band 5 must be either 14 or 13 as a $\Delta I = 3$ transition is highly improbable. The levels populated in band 6 are 13^+ and 12^+, which also solidifies the fact that the lowest level in band 5 must be either 14 or 13. However, a spin 14 assignment would result in either the 1065- or the 989-keV γ ray being of $M2$ character, an unlikely proposition. Thus, the lowest level in band 5 has been assigned a spin of $13\hbar$, with the negative parity proposed being based upon its configuration assignment (see Sec. IV E).

B. Positive-parity bands

The strongly coupled structure labeled band 6 in Fig. 2 was previously observed and associated with a positive-parity configuration [4]. Arguments for the spin assignments were previously made using the additivity of alignment method [4] and were regarded as tentative. The intensity of band 6 is similar to that of bands 1 and 2, indicating that all three are relatively close in energy. This is consistent with the excitation energy plots of Figs. 5(a) and 5(b). If a different spin were assumed, the energy of band 6 would be either much higher or lower than those of bands 1 and 2, and it would be inconsistent with the observed intensities. Therefore, we are in agreement with the proposed spins of Zhang *et al.* [4], as well as their parity assignment, the latter being based upon the configuration (see Sec. IV F). Two new transitions (89 and 211 keV) were added below the previously observed lowest state (8^+), and the band was extended from $I = 23\hbar$ to $49\hbar$, the highest spin observed in the nucleus. A spectrum displaying both signatures of band 6 is provided in Fig. 7(a).

Band 7 is a new strongly coupled structure that feeds band 6 at low spins with a series of six $\Delta I = 1$ transitions and one $\Delta I = 2$ transition. The angular correlation ratios of three linking transitions were obtained. The ratios of the 226- and 282-keV transitions are 0.64(7) and 0.67(6), respectively; these are consistent with the γ rays being of stretched dipole character. The ratio of the 404-keV transition was found to be 1.04(10), consistent with a stretched quadrupole character. Thus, band 7 has the same parity (positive) as band 6, and the relative spins for the former can be confidently assigned as proposed in Fig. 2. A spectrum displaying the sequence is shown in Fig. 7(b). In addition, three sequences of presumed $E2$ transitions were found to primarily feed band 7 and are labeled as bands 8, 9, and 8a in Fig. 2. The linking transitions were assumed to be of $E2$ character such that the states that feed into band 7 ($I = 21\hbar$, $22\hbar$, and $23\hbar$) are nearly degenerate with levels in the same structure [see Fig. 5(b)].

TABLE I. Summary of the spectroscopic information for ^{170}Ta excitations in the present work.

I^{π} [a]	E_{level} (keV)[b]	E_{γ} [c]	T_{γ} [d]	Ang. Corr. Ratio
Band 1 ($\alpha = 1$)				
9^-	268.3	122.7	5.9	
9^-	268.3	211.6	5.9	0.67(2)
11^-	496.7	130.9	3.8	0.68(3)
11^-	496.7	228.4	5.9	
13^-	855.0	156.3	1.5	
13^-	855.0	191.4	40.6	0.67(2)
13^-	855.0	358.3	20.6	0.96(6)
15^-	1320.6	218.6	1.2	
15^-	1320.6	242.3	35.3	0.68(3)
15^-	1320.6	465.6	29.4	0.92(5)
17^-	1872.8	274.7	1.4	
17^-	1872.8	285.1	17.6	0.66(5)
17^-	1872.8	552.2	26.5	1.12(7)
19^-	2494.9	324.2	5.9	
19^-	2494.9	585.1	16.5	1.10(3)
19^-	2494.9	622.1	11.8	
21^-	3142.6	340.5	7.9	0.64(2)
21^-	3142.6	647.7	9.4	
21^-	3142.6	660.2	2.9	
23^-	3806.1	348.5	5.9	0.63(3)
23^-	3806.1	663.5	6.5	
25^-	4495.5	366.1	5.9	0.59(4)
25^-	4495.5	689.4	4.1	
27^-	5243.3	400.0	2.1	
27^-	5243.3	747.8	3.5	
29^-	6065.1	444.0	1.8	
29^-	6065.1	821.8	3.4	
31^-	6960.6	895.5	1.9	
33^-	7938.6	956.4	0.3	
33^-	7938.6	978.0	0.6	
35^-	8976.3	1037.7	0.2	
37^-	10084.5	1108.1	0.1	
39^-	11235.3	1150.8	0.1	
Band 1 ($\alpha = 0$)				
8^-	145.6	88.9	5.9	
10^-	365.7	97.4	5.9	0.52(6)
12^-	663.4	167.0	18.8	0.65(2)
12^-	663.4	297.7	5.9	
14^-	1078.4	223.6	32.4	0.71(2)
14^-	1078.4	415.0	17.6	0.98(4)
16^-	1587.5	266.9	26.5	0.68(3)
16^-	1587.5	509.1	26.5	0.88(3)
18^-	2170.3	297.6	14.7	
18^-	2170.3	582.8	25.9	0.99(4)
20^-	2801.7	307.0	5.9	
20^-	2801.7	319.3	5.9	0.58(3)
20^-	2801.7	626.6	1.0	
20^-	2801.7	631.4	21.2	
22^-	3457.1	315.0	6.9	0.60(4)
22^-	3457.1	655.4	12.9	1.03(4)
24^-	4129.0	323.6	3.8	0.73(6)
24^-	4129.0	671.9	6.8	1.11(5)
26^-	4842.6	347.7	3.0	
26^-	4842.6	713.6	5.9	
28^-	5620.5	377.7	1.8	
28^-	5620.5	777.9	3.6	
30^-	6467.5	847.0	1.8	
32^-	7380.0	912.5	0.7	
34^-	8351.1	971.1	0.4	
36^-	9370.5	1019.4	0.6	
38^-	10430.1	1059.6	0.5	
40^-	11519.3	1089.2	0.2	
42^-	12639.3	1120.0	0.1	
44^-	13792.7	1153.4	<0.1	
46^-	14976.8	1184.1	<0.1	
48^-	16195.8	1219.0	<0.1	
Band 2 ($\alpha = 0$)				
8^-	182.7	50.8		
8^-	182.7	136.5	5.9	0.63(11)
10^-	394.0	71.5	2.4	
10^-	394.0	211.3	5.9	1.02(8)
12^-	698.7	103.0	4.7	
12^-	698.7	304.7	100.0	0.86(2)
14^-	1102.0	147.1	4.7	
14^-	1102.0	247.0	3.1	
14^-	1102.0	403.3	79.4	0.94(4)
16^-	1598.1	277.5	2.9	
16^-	1598.1	496.1	58.8	1.00(5)
18^-	2175.1	577.0	35.3	0.97(5)
20^-	2821.7	646.6	17.6	1.04(6)
22^-	3526.0	704.3	7.6	1.04(6)
24^-	4280.8	754.8	5.3	1.10(7)
26^-	5081.5	800.7	3.2	0.98(7)
28^-	5924.6	843.1	2.1	0.87(7)
30^-	6814.9	890.3	1.8	
32^-	7756.3	941.4	0.9	
34^-	8753.2	996.9	0.3	
36^-	9810.9	1057.7	0.2	
38^-	10882.6	1071.7	0.1	
Band 2 ($\alpha = 1$)				
7^-	131.9	85.7	2.4	
9^-	322.5	139.8	5.9	0.54(2)
9^-	322.5	190.6	11.8	0.88(5)
11^-	595.7	201.7	29.4	0.50(2)
11^-	595.7	273.2	24.1	0.84(2)
13^-	954.9	256.2	24.7	0.45(2)
13^-	954.9	359.2	32.9	0.92(3)
15^-	1395.3	293.3	17.6	
15^-	1395.3	316.9	0.2	
15^-	1395.3	440.4	32.4	0.93(9)
17^-	1909.8	311.7	13.5	
17^-	1909.8	322.3	3.1	
17^-	1909.8	514.5	29.4	0.84(2)
19^-	2482.4	307.3	5.9	
19^-	2482.4	312.1	5.9	
19^-	2482.4	572.6	15.3	1.04(3)
19^-	2482.4	609.6	14.1	0.82(4)
21^-	3119.5	297.8	2.4	
21^-	3119.5	317.8	0.2	
21^-	3119.5	624.6	3.2	
21^-	3119.5	637.1	14.7	1.18(7)

TABLE I. (*Continued.*)

I^{π} [a]	E_{level} (keV)[b]	E_{γ} [c]	T_{γ} [d]	Ang. Corr. Ratio
23^-	3799.0	273.0	1.4	
23^-	3799.0	679.5	11.2	1.07(6)
25^-	4520.9	240.1	0.3	
25^-	4520.9	721.9	8.2	
27^-	5287.5	766.6	6.5	
29^-	6105.6	818.1	3.2	
31^-	6982.2	876.6	1.2	
33^-	7908.3	926.1	0.9	
33^-	7908.3	947.7	0.6	
35^-	8901.8	993.5	0.9	
37^-	9949.7	1047.9	0.6	
39^-	11047.2	1097.5	0.3	
41^-	12193.7	1146.5	0.1	
43^-	13361.5	1167.7	0.1	
Band 3				
8^-	434.9	228.1	11.8	
8^-	434.9	303.0	1.8	
10^-	719.3	284.4	11.8	0.93(4)
10^-	719.3	396.8	4.1	0.51(4)
12^-	1068.5	349.2	8.8	0.88(6)
12^-	1068.5	472.9	3.5	0.50(4)
14^-	1491.1	422.6	11.8	0.98(4)
14^-	1491.1	536.0	2.4	0.61(7)
16^-	1987.5	496.4	8.8	1.08(5)
16^-	1987.5	592.0	1.2	
18^-	2551.2	563.7	7.1	0.91(5)
20^-	3169.0	617.8	5.0	0.94(5)
22^-	3824.6	655.6	3.4	0.97(6)
24^-	4510.7	686.1	1.6	1.07(7)
26^-	5267.3	756.6	0.9	
28^-	6068.5	801.2	0.4	
30^-	6906.8	838.3	0.3	
32^-	7796.1	889.5	0.1	
Band 4				
24^-	4526.1	701.5	1.8	
26^-	5229.3	703.2	1.2	
28^-	5973.2	743.9	0.6	
30^-	6767.5	794.3	0.6	
32^-	7622.3	854.9	0.5	
34^-	8537.6	915.2	0.5	
36^-	9513.2	975.6	0.2	
38^-	10549.9	1036.7	0.1	
40^-	11648.6	1098.7	0.1	
Band 5 ($\alpha = 1$)				
13^-	1728.6	442.1	0.6	
13^-	1728.6	650.2	0.5	
13^-	1728.6	773.8	0.4	
13^-	1728.6	873.6	0.4	
13^-	1728.6	989.1	0.9	
13^-	1728.6	1065.2	0.3	
15^-	2144.5	239.9	14.7	
15^-	2144.5	415.9	0.6	
17^-	2737.1	311.0	8.8	
17^-	2737.1	592.6	0.6	
19^-	3416.5	346.9	3.5	
19^-	3416.5	679.4	0.6	
21^-	4110.3	346.9	1.8	
21^-	4110.3	693.8	0.6	
Band 5 ($\alpha = 0$)				
14^-	1904.6	176.0	5.9	
16^-	2426.1	281.6	10.6	
16^-	2426.1	521.5	0.6	
18^-	3069.6	332.5	7.1	
18^-	3069.6	643.5	0.6	
20^-	3763.4	346.9	2.4	
20^-	3763.4	693.8	0.6	
22^-	4475.9	365.6	1.8	
22^-	4475.9	712.5	0.6	
Band 6 ($\alpha = 0$)				
8^+	89.3	89.3	5.9	0.69(10)
10^+	362.6	152.0	13.9	0.70(2)
10^+	362.6	273.3	11.8	0.90(4)
12^+	739.5	203.1	17.6	0.70(2)
12^+	739.5	376.9	17.6	0.97(3)
14^+	1201.6	246.8	20.6	0.66(2)
14^+	1201.6	462.1	38.2	0.97(4)
16^+	1732.1	281.7	17.6	0.74(5)
16^+	1732.1	530.5	35.3	1.04(3)
18^+	2312.5	306.8	11.5	0.66(3)
18^+	2312.5	580.4	29.4	0.94(3)
20^+	2924.5	323.6	4.7	
20^+	2924.5	612.0	20.0	0.94(3)
22^+	3559.7	340.4	6.5	0.61(3)
22^+	3559.7	635.2	9.7	1.14(4)
24^+	4231.0	366.1	5.0	0.68(4)
24^+	4231.0	671.3	7.5	0.97(4)
26^+	4958.1	398.4	2.9	
26^+	4958.1	727.1	6.1	1.02(7)
28^+	5747.3	428.9	1.8	
28^+	5747.3	789.2	4.4	0.97(9)
30^+	6595.5	452.8	0.9	
30^+	6595.5	848.2	4.2	
32^+	7499.5	469.8	0.4	
32^+	7499.5	904.0	2.4	
34^+	8456.6	957.1	1.5	
36^+	9459.3	1002.7	1.2	
38^+	10500.8	1041.5	0.7	
40^+	11584.2	1083.4	0.4	
42^+	12712.8	1128.6	0.2	
44^+	13889.1	1176.3	0.1	
46^+	15106.0	1216.9	<0.1	
Band 6 ($\alpha = 1$)				
9^+	210.9	121.5	3.4	0.61(3)
9^+	210.9	210.9	8.8	
11^+	536.3	173.8	14.7	0.69(2)
11^+	536.3	325.4	14.7	
13^+	954.8	215.4	23.5	0.64(3)
13^+	954.8	418.5	38.2	1.00(4)
15^+	1450.3	248.7	18.8	0.82(16)
15^+	1450.3	495.5	35.3	0.96(2)
17^+	2005.5	273.4	17.6	0.76(3)
17^+	2005.5	555.2	32.4	0.93(3)

TABLE I. (*Continued.*)

I^{π} [a]	E_{level} (keV)[b]	E_{γ} [c]	T_{γ} [d]	Ang. Corr. Ratio
19^+	2600.7	288.2	11.8	0.72(4)
19^+	2600.7	595.2	29.4	0.91(3)
21^+	3219.3	294.8	8.2	0.72(3)
21^+	3219.3	618.6	22.9	1.13(4)
23^+	3864.9	305.0	4.1	0.60(5)
23^+	3864.9	645.6	13.5	1.14(4)
25^+	4559.5	328.7	3.5	
25^+	4559.5	694.6	10.6	1.16(6)
27^+	5318.1	360.0	2.4	
27^+	5318.1	758.6	7.6	1.02(8)
29^+	6142.8	395.4	0.9	
29^+	6142.8	824.7	5.0	
31^+	7030.0	434.6	1.0	
31^+	7030.0	887.2	3.1	
33^+	7959.2	869.5	0.3	
33^+	7959.2	929.2	2.2	
35^+	8904.1	944.9	1.5	
37^+	9906.8	1002.7	1.0	
39^+	10971.2	1064.4	0.5	
41^+	12092.1	1120.9	0.3	
43^+	13260.8	1168.7	0.2	
45^+	14458.1	1197.3	0.1	
47^+	15688.8	1230.7	<0.1	
49^+	16955.8	1267.0	<0.1	
Band 7 ($\alpha = 1$)				
9^+	291.4	110.4	2.9	
9^+	291.4	202.1	1.8	
11^+	614.5	177.9	8.8	0.79(6)
11^+	614.5	252.0	4.7	
11^+	614.5	323.1	29.4	1.03(6)
11^+	614.5	403.7	5.9	1.04(10)
13^+	1047.5	228.7	7.6	
13^+	1047.5	308.2	1.5	
13^+	1047.5	433.0	26.5	0.95(4)
15^+	1563.1	265.9	5.9	
15^+	1563.1	515.6	23.5	1.11(4)
17^+	2137.4	290.7	2.4	
17^+	2137.4	574.3	20.6	1.08(5)
19^+	2748.0	303.6	1.1	
19^+	2748.0	610.6	11.8	1.24(10)
21^+	3376.9	307.9	1.2	
21^+	3376.9	628.9	6.5	1.09(6)
23^+	3996.6	313.9	1.2	
23^+	3996.6	601.6	0.6	
23^+	3996.6	619.7	2.4	
23^+	3996.6	777.1	1.8	
25^+	4673.8	349.3	1.2	
25^+	4673.8	677.2	2.9	
27^+	5421.9	381.8	1.2	
27^+	5421.9	748.1	1.8	
29^+	6233.0	811.1	1.2	
31^+	7089.7	856.7	1.2	
33^+	7994.6	904.9	0.4	
35^+	8996.2	1001.6	0.2	
Band 7 ($\alpha = 0$)				
10^+	436.8	145.4	11.8	0.94(9)

TABLE I. (*Continued.*)

I^{π} [a]	E_{level} (keV)[b]	E_{γ} [c]	T_{γ} [d]	Ang. Corr. Ratio
10^+	436.8	225.7	5.9	0.64(7)
10^+	436.8	255.9	35.3	0.72(6)
12^+	818.8	204.3	11.8	1.04(7)
12^+	818.8	282.3	5.3	0.67(6)
12^+	818.8	382.0	30.0	0.87(3)
14^+	1297.0	249.6	8.8	
14^+	1297.0	342.2	5.3	
14^+	1297.0	478.2	29.4	0.92(4)
16^+	1846.5	283.8	2.4	
16^+	1846.5	549.5	21.2	0.96(4)
18^+	2444.3	307.2	0.3	
18^+	2444.3	597.8	14.7	1.05(4)
20^+	3069.0	321.0	1.2	
20^+	3069.0	624.7	7.6	1.00(5)
22^+	3683.0	306.0	2.1	
22^+	3683.0	529.3	0.6	
22^+	3683.0	614.0	2.9	
24^+	4324.8	328.0	1.2	
24^+	4324.8	641.8	1.6	
26^+	5040.5	366.2	1.2	
26^+	5040.5	715.7	1.2	
28^+	5826.5	404.3	0.6	
28^+	5826.5	786.0	1.1	
30^+	6681.4	854.9	0.6	
32^+	7602.4	921.0	0.2	
34^+	8583.9	981.5	0.2	
36^+	9588.0	1004.1	0.1	
Band 8				
20^+	3153.7	709.4	0.6	
22^+	3743.0	589.3	1.2	
22^+	3743.0	674.0	2.9	
24^+	4434.8	691.8	1.9	
26^+	5188.9	754.1	0.8	
28^+	5984.3	795.4	0.3	
30^+	6814.0	829.7	0.1	
32^+	7687.9	873.9	<0.1	
34^+	8623.2	935.3	<0.1	
Band 8a				
28^+	6027.3	838.4	0.2	
30^+	6921.0	893.8	0.1	
32^+	7858.3	937.3	<0.1	
34^+	8807.5	949.2	<0.1	
Band 9				
21^+	3420.0	672.0	1.2	
23^+	4072.5	652.5	0.6	
23^+	4072.5	677.5	1.8	
23^+	4072.5	695.6	0.9	
25^+	4794.2	721.7	1.5	
27^+	5578.2	784.0	0.5	
29^+	6430.6	852.4	0.4	
31^+	7331.9	901.3	0.4	
33^+	8280.2	948.3	0.2	
Band 10 ($\alpha = 1$)				
7^+	211.0	178.6	5.9	
9^+	473.0	133.4	0.6	
9^+	473.0	262.0	5.9	0.76(6)

TABLE I. (*Continued.*)

I^{π} [a]	E_{level} (keV)[b]	E_{γ} [c]	T_{γ} [d]	Ang. Corr. Ratio
11^+	810.0	172.6	2.9	
11^+	810.0	183.8	2.9	
11^+	810.0	273.7	1.2	
11^+	810.0	337.0	8.8	0.81(4)
11^+	810.0	347.3	11.8	0.83(4)
13^+	1223.3	406.4	5.9	
13^+	1223.3	413.3	21.2	0.93(4)
15^+	1696.0	472.7	17.6	0.92(3)
17^+	2220.0	524.0	13.5	1.12(4)
17^+	2220.0	575.0	1.1	
19^+	2782.8	562.8	9.4	0.99(4)
19^+	2782.8	579.8	3.8	1.00(5)
21^+	3395.0	612.2	8.5	0.99(5)
23^+	4056.0	661.0	2.9	1.19(10)
23^+	4056.0	679.1	1.8	
25^+	4777.5	721.5	2.6	1.04(9)
27^+	5542.2	764.7	1.6	
29^+	6320.4	778.2	1.0	
31^+	7158.0	837.6	0.7	
33^+	8091.5	933.5	0.5	
35^+	9097.2	1005.7	0.2	
37^+	10164.1	1066.9	0.1	
39^+	11277.5	1113.4	<0.1	
41^+	12446.8	1169.4	<0.1	
Band 10 ($\alpha = 0$)				
8^+	328.2	217.4	8.8	
10^+	626.2	263.6	5.9	
10^+	626.2	298.0	14.1	0.80(3)
12^+	1010.7	174.9	2.4	
12^+	1010.7	384.5	12.9	0.89(3)
14^+	1462.0	451.3	12.4	0.95(2)
16^+	1981.5	519.5	11.8	1.08(6)
16^+	1981.5	551.0	6.5	1.06(5)
18^+	2566.5	585.0	8.8	1.05(3)
20^+	3181.3	614.8	5.9	1.11(4)
22^+	3804.0	622.7	2.9	1.22(5)
24^+	4470.0	666.0	1.2	0.93(6)
24^+	4470.0	690.5	1.2	
26^+	5207.7	737.7	0.5	
28^+	6026.7	819.0	0.4	
30^+	6920.3	893.6	0.3	
Band 10a				
	3879.5	698.2	1.2	
	4564.2	684.7	0.6	
	5314.3	750.1	0.3	
Band 10b				
	6417.5	875.3	0.2	
	7311.3	893.8	0.2	
	8260.7	949.4	0.2	
	9258.5	997.8	0.1	
Low-spin levels fed by band 10				
	339.5	250.5	5.9	
	462.5	123.0	1.2	
	637.4	174.9	1.2	
	637.4	297.9	2.9	

TABLE I. (*Continued.*)

I^{π} [a]	E_{level} (keV)[b]	E_{γ} [c]	T_{γ} [d]	Ang. Corr. Ratio
	626.4	164.1	5.9	
	816.9	179.3	5.9	
	816.9	190.5	5.9	
	816.9	343.7	5.9	
	816.9	354.6	5.9	
Band 11 ($\alpha = 1$)				
7^+	170.9	170.8	5.9	0.80(10)
9^+	395.0	83.0	5.9	
9^+	395.0	224.1	17.6	0.78(3)
9^+	395.0	305.8	8.8	0.76(6)
11^+	723.7	139.1	1.8	
11^+	723.7	328.7	20.6	0.86(3)
11^+	723.7	361.2	2.9	
13^+	1145.4	182.8	1.8	
13^+	1145.4	406.0	1.8	
13^+	1145.4	421.7	17.6	0.98(3)
15^+	1645.0	499.6	14.7	0.99(3)
17^+	2203.0	507.0	1.4	
17^+	2203.0	558.0	11.8	1.00(3)
19^+	2810.2	590.1	2.9	
19^+	2810.2	607.2	4.4	1.07(6)
21^+	3449.5	639.3	2.9	1.17(9)
23^+	4118.9	669.4	2.2	1.09(14)
25^+	4835.1	716.2	0.6	
27^+	5599.5	764.4	0.4	
29^+	6405.6	806.1	0.2	
31^+	7258.5	852.9	0.1	
33^+	8150.4	891.9	<0.1	
35^+	9070.8	920.4	<0.1	
Band 11 ($\alpha = 0$)				
8^+	312.0	222.9	2.4	0.75(7)
8^+	312.0	312.0	1.8	0.58(5)
10^+	584.6	260.7	5.9	0.72(4)
10^+	584.6	272.6	23.5	0.84(2)
12^+	962.6	222.9	3.5	
12^+	962.6	378.0	20.6	0.96(3)
14^+	1430.3	467.7	17.6	0.96(4)
16^+	1956.8	494.8	5.9	0.81(7)
16^+	1956.8	526.5	14.7	0.98(3)
18^+	2517.1	535.6	1.5	
18^+	2517.1	560.3	11.8	1.14(5)
20^+	3122.9	605.8	8.8	0.98(5)
22^+	3779.1	656.2	6.5	1.08(7)
24^+	4493.6	689.6	0.5	
24^+	4493.6	714.5	3.8	1.09(12)
26^+	5256.9	763.3	2.5	0.89(8)
28^+	6080.7	823.8	1.3	
30^+	6949.5	868.8	0.6	
32^+	7870.6	921.1	0.6	
34^+	8844.4	973.8	0.5	
36^+	9864.8	1020.4	0.3	
38^+	10920.3	1055.5	0.2	
Band 11a				
	6052.4	795.5	0.5	
	6863.7	811.3	0.3	
	7757.2	893.5	0.1	

TABLE I. (*Continued.*)

I^{π} [a]	E_{level} (keV)[b]	E_{γ} [c]	T_{γ} [d]	Ang. Corr. Ratio
Band 11b				
	3144.3	627.2	1.2	
	3834.3	690.0	1.2	
	4579.0	744.7	1.2	
	5389.5	810.5	0.9	
Low-spin levels fed by band 11				
	323.9	234.8	5.9	
	323.9	323.9	5.9	

[a]Spin and parity of the depopulated state. The spin and parity values are based on angular correlation ratios, level interactions, and configuration assignments.

[b]Absolute energy levels are not known. Relative energy levels are with respect to the lowest observed state in the level scheme, the 7^{+} state in band 6.

[c]Uncertainties in γ-ray energy are 0.2 keV for most transitions, except for relatively weak transitions ($I_{\gamma} < 1$) where 0.5 keV uncertainties are appropriate.

[d]Relative intensity of the transition with respect to the intensity ($I \equiv 100$) of the 304.7-keV transition in band 2. Uncertainties for stronger transitions (>5) is less than 5%, whereas those for weaker transitions (<5) are approximately 10%.

Bands 10 and 11 are two sets of semidecoupled sequences that also strongly interact with each other. Sample spectra for these two bands are provided in Fig. 8. The $\alpha = 0, 1$ signatures of these bands were determined to be partners by examining their similarities in both the excitation energy plot [Fig. 5(c)] and the alignment plot [Figs. 9(e) and 9(f)]. The relative spins and parity of band 11 were determined by examining the angular correlation ratios of the transitions feeding into band 6. The ratios of these linking transitions were determined to be 0.8(1) (171 keV), 0.72(4) (261 keV), 0.76(6) (306 keV), and 0.58(5) (312 keV), respectively. The 261-, 306-, and 312-keV transitions all have angular correlation ratios consistent with $\Delta I = 1$ transitions, whereas the 171-keV transition is consistent with a $\Delta I = 0$ transition. This allows for a confident spin assignment to band 11 with the range of energy levels going from $I = 7\hbar$ to $38\hbar$. Although band 10 directly feeds band 6, the intensities of the feeding transitions are too low to obtain angular correlation ratios. However, since spin assignments were made for band 11, the linking transitions between bands 10 and 11 can be used to assign the relative spins and energy of band 10. The angular correlation ratios of the 551- and 580-keV linking transitions [1.06(5) and 1.00(6), respectively] are consistent with a quadrupole character. Thus, a relative spin/parity assignment can be proposed where the lowest and highest spin states are found to have $I^{\pi} = 5^{+}$ and 41^{+} quantum numbers. The parities for both bands are likely to be positive as they feed into another positive-parity structure. This assignment is consistent with the configurations proposed (see the following). Several short sequences were found feeding into bands 10 and 11, and these are labeled as 10a, 10b, 11a, and 11b in Fig. 3.

IV. DISCUSSION

Various techniques were used to assign configurations to the many bands in ^{170}Ta. The observed quasiproton and quasineutron orbitals in ^{169,171}Ta [15,16], ^{169}Hf [21], and ^{171}W [22]) were considered. There are many quasiproton excitations seen at low energy and these include $d_{5/2}[402]5/2$, $g_{7/2}[404]7/2$, $d_{3/2}[411]1/2$, $h_{9/2}[541]1/2$, and $h_{11/2}[514]9/2$. The quasineutron orbitals that have been observed are $h_{9/2}[523]5/2$, $f_{7/2}[512]5/2$, and $i_{13/2}[642]5/2$. However, the $vi_{13/2}$ bands typically lie much lower in energy (~300–400 keV) than the negative-parity structures in the low-spin ($7\hbar$–$15\hbar$) region. A detailed analysis of the observed alignment and Routhian behavior of the ^{170}Ta bands was performed along with a comparison of the extracted $B(M1)/B(E2)$ values with theoretical predictions, when possible. Since the alignments and band crossings will be interpreted within the framework of the cranked shell model (CSM) [23], the following alphabetic labeling system has been applied: $(\pi, \alpha) = (+, +1/2)$ A, C, I; $(+, -1/2)$ B, D, J; $(-, +1/2)$ E, G; $(-, -1/2)$ F, H, where the first letter represents the configuration initially lowest in energy for the given (π, α) quantum numbers. The labels assigned to the Nilsson orbitals (at $\hbar\omega = 0$) can be found in Table II, where a subscript p denotes a quasiproton. Figure 9 presents the alignments for bands 1–11 in ^{170}Ta, where a reference was subtracted using Harris parameters [24] of $\mathcal{J}_0 = 28\ \hbar^2/\text{MeV}$ and $\mathcal{J}_1 = 58\ \hbar^4/\text{MeV}^3$ that were selected to produce a nearly zero initial alignment at low frequency and a constant alignment above the first band crossing in ^{168}Hf [25].

CSM calculations were also performed to help assign configurations by interpreting the observed band crossings. The five-point fit defined in Ref. [26] gives proton and neutron pairing energies of 1.11 and 1.06 MeV, respectively, and these values were used in the CSM calculations. Quasiproton and quasineutron Routhian diagrams are given in Figs. 10 and 11 with the different crossings indicated. In particular, one may note that the BC neutron crossing is predicted to be at 0.31 MeV. It is this crossing that is observed in nearly all of the bands in ^{170}Ta (Fig. 9). The predicted alignment gain, Δi_x, for the BC crossing, the derivative of the Routhian, is $\sim 7\hbar$, a value that is consistent with the experimentally measured ones.

Branching ratios were determined whenever possible using

$$\lambda = \frac{T_{\gamma}(I \to I-2)}{T_{\gamma}(I \to I-1)}, \tag{1}$$

where $T_{\gamma}(I \to I-2)$ corresponds to the γ-ray intensity of the $\Delta I = 2$ transition, and $T_{\gamma}(I \to I-1)$ is the corresponding intensity of the $\Delta I = 1$ transition. These intensities were measured by gating on transitions above the state of interest and may differ slightly from the intensity values listed in Table I. The branching ratios can be used to directly calculate the relative transition probabilities defined as

$$\frac{B(M1: I \to I-1)}{B(E2: I \to I-2)} = 0.697 \frac{1}{\lambda} \frac{E_{\gamma}^{5}(I \to I-2)}{E_{\gamma}^{3}(I \to I-1)} \frac{1}{(1+\delta^2)}, \tag{2}$$

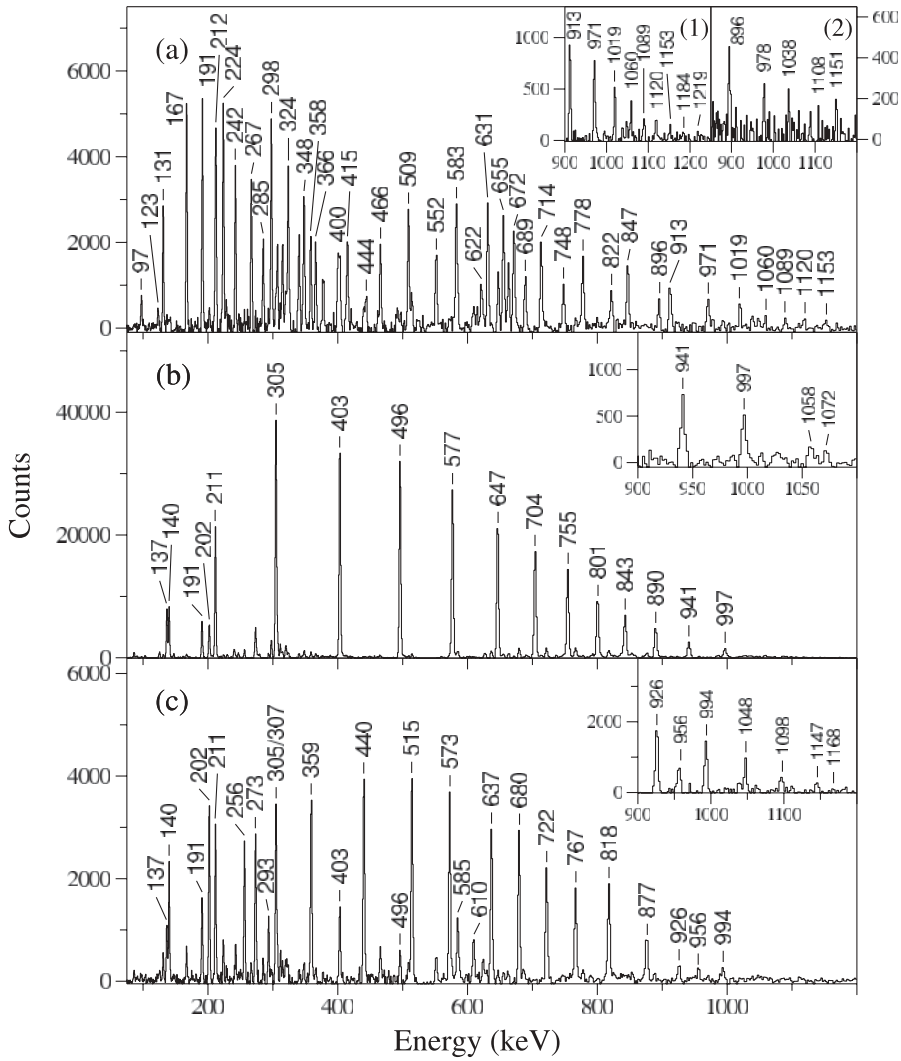

FIG. 4. Coincidence spectra for (a) both signatures of band 1, (b) the $\alpha = 0$ signature of band 2, and (c) the $\alpha = 1$ signature of band 2. All spectra were produced by summing as many clean triple coincidence gates of the inband transitions as possible from a hypercube. The insets in each panel display the highest possible energy regions.

where $E_\gamma(I \to I-2)$ and $E_\gamma(I \to I-1)$ are the $\Delta I = 2$ and $\Delta I = 1$ transition energies, and δ is the $E2/M1$ mixing ratio for the $\Delta I = 1$ transitions. Mixing ratios were estimated from the rotational model and assumed pure K values [27]. The theoretical values were calculated using the geometric model of Dönau and Frauendorf [28]. The g_R value was taken to be Z/A and the g_Ω values were calculated using a Woods-Saxon potential. Table II lists the parameters used in the present calculations. The intrinsic quadrupole moment of the nucleus ($Q_0 = 7.0\ e$ b) is taken as the average of the even-even neighbors of ^{170}Ta [4]. The experimental $B(M1)/B(E2)$ ratios are compared in Figs. 12 and 13 with the theoretical predictions (denoted by the various lines).

There are two ways for the valence quasiproton and valence quasineutron to couple: with intrinsic spins parallel or antiparallel. According to the Gallagher-Moszkowski (G-M) rules [29], the parallel coupling lies lower than the antiparallel one (at the bandhead) with a splitting of 50 to 200 keV. The preferred K value of the band is also determined using G-M rules where

$$K = \begin{cases} K_p + K_n & \text{if } j_p = l_p \pm \frac{1}{2}, \quad j_n = l_n \pm \frac{1}{2}, \\ |K_p - K_n| & \text{if } j_p = l_p \pm \frac{1}{2}, \quad j_n = l_n \mp \frac{1}{2}. \end{cases} \tag{3}$$

In most cases, the splitting between the parallel and antiparallel coupling is too large to observe both bands. However, there are cases in nearby nuclei where both couplings have been observed. (See, for example, Reviol *et al.* [10].)

A. Band 1: $\pi h_{11/2} \nu i_{13/2}$

The alignment for band 1, shown in Fig. 9(a), displays a gain of $\Delta i_x \approx 7\hbar$ near $\hbar\omega = 0.31$ MeV. This value is smaller and the alignment occurs at a higher frequency than the AB

TABLE II. Parameters used in calculating theoretical $B(M1)/B(E2)$ values shown in Figs. 12 and 13.

Configuration	K	g_Ω	i_x
$\pi 5/2[402](A_pB_p)$	2.5	1.57	0.0
$\pi 7/2[404](C_pD_p)$	3.5	0.61	0.0
$\pi 9/2[514](E_pF_p)$	4.5	1.30	1.6
$\pi 1/2[541](G_pH_p)$	0.5	1.11	3.0
$\pi 1/2[411](I_pJ_p)$	0.5	−1.23	0.0
$\nu 5/2[642](A, B)$	2.5	−0.30	5.0, 4.0
$\nu 5/2[523](E, F)$	2.5	−0.38	1.0
νBC	0.0	−0.30	7.3

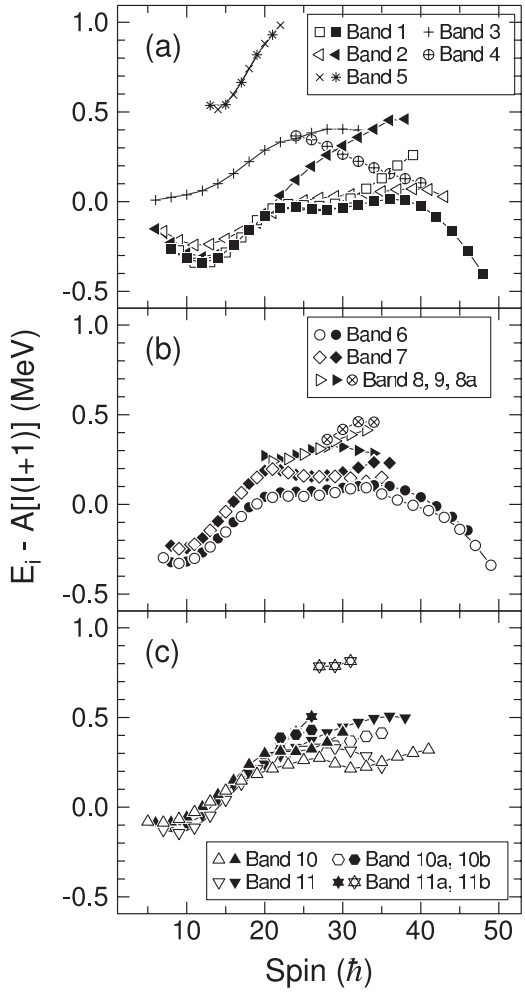

FIG. 5. Excitation energy minus a rigid-rotor reference (where $A = 0.0071$ MeV) for (a) all negative-parity bands in ^{170}Ta, (b) bands 6, 7, 8, 8a, and 9, and (c) bands 10, 10a, 10b, 11, 11a, and 11b. Filled (empty) symbols denote the $\alpha = 0$ (1) signatures.

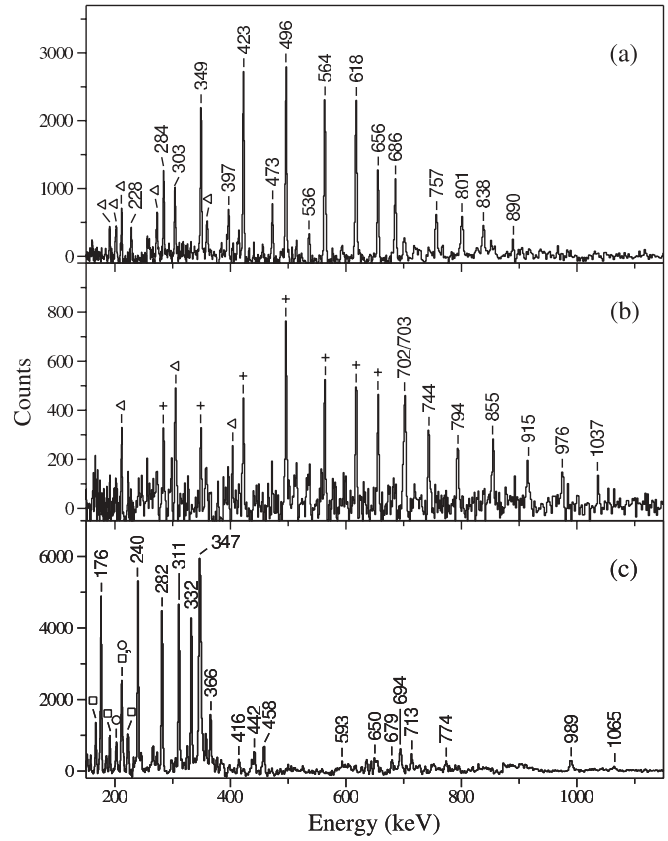

FIG. 6. Representative spectra of bands (a) 3, (b) 4, and (c) 5 obtained as a result of summing all triple-gated coincidence spectra using inband transitions. In panels (a) and (b), the open left triangles denote peaks from band 2. The plus signs in panel (b) represent peaks assigned to band 3, and the open squares and circles in panel (c) are transitions in bands 1 and 6, respectively.

crossing seen in ^{168}Hf, suggesting that the AB alignment is blocked in band 1. Indeed, the CSM calculations, as already discussed, predict that the BC crossing should occur at 0.31 MeV. Thus, the A quasineutron (associated with the $\nu i_{13/2}$ orbital) must be involved in the configuration of this band. The $B(M1)/B(E2)$ ratios for band 1 are plotted in Fig. 12, and a satisfactory fit with the theoretical values for the $\pi h_{11/2}\nu i_{13/2}$ configuration (line 1) is observed. Based upon these results, we assign the E_pA and F_pA configurations to the $\alpha = 1$ and 0 sequences, respectively, and $K^\pi = 7^-$ can be associated with the bandhead. This is in agreement with the interpretation of Zhang *et al.* [4]. It is also consistent with the fact that band 1 is yrast in ^{170}Ta as are the $\pi h_{11/2}$ bands in the neighboring Ta nuclei and the $\nu i_{13/2}$ band in the neighboring odd-N nuclei.

At higher frequencies, the F_pA sequence experiences another crossing at ~0.52 MeV and gains approximately $5\hbar$ in alignment. The CD crossing is blocked following the BC alignment, and it is highly unlikely that the EF crossing would produce an alignment gain this large. Therefore, this high-frequency crossing may be the result of a quasiproton alignment, although the character of the quasiprotons involved is not necessarily clear. A crossing is observed near 0.55 MeV in the ground-state band of ^{168}Hf and was interpreted as a mixed $h_{11/2}/h_{9/2}$ (F_pG_p) quasiproton alignment [25]. This F_pG_p alignment would be blocked in the F_pA sequence, and this interpretation does not fit the observed crossing in ^{170}Ta. The E_pH_p crossing is a possible interpretation; however, one would expect to observe the F_pG_p alignment in the E_pA signature at a lower frequency, but no such high-frequency crossing is observed in the odd-spin sequence as seen in Fig. 9(a). Another explanation may be that this corresponds to the G_pH_p crossing, but once again, a crossing at the same frequency should be present in the E_pA structure. There is no evidence of any such crossing in the latter sequence; however, this structure does mix with the G_pA configuration (band 2) at $I = 31\hbar$ (see Fig. 1) and these bands lie close in energy over a significant spin range [see Fig. 5(a)]. As a result of this mixing, it is possible that any crossing involving an $h_{9/2}$ quasiproton is blocked in the E_pA sequence. Finally, it is also possible that the alignment gain in the F_pA sequence results from a crossing with band 4. As can be seen in Fig. 5(a), there may be an interaction between the bands near $I = 40\hbar$, and, perhaps, they exchange character. The observation of linking transitions between the structures would provide further evidence for this

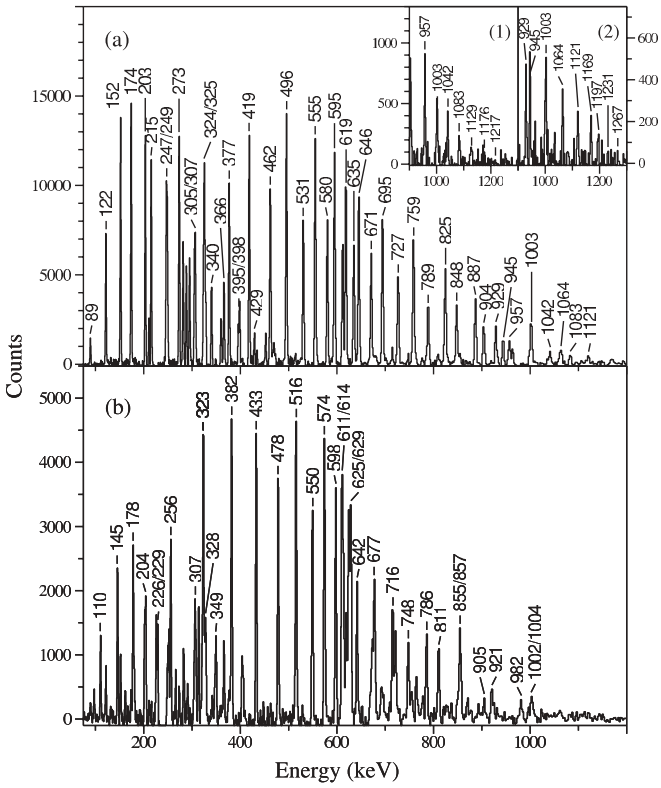

FIG. 7. Coincidence spectra for bands (a) 6 and (b) 7. These spectra were generated in the same format as that described in Figs. 4 and 6. Insets (1) and (2) in panel (a) display the highest spin portions for the $\alpha = 0$ and 1 signatures of band 6, respectively.

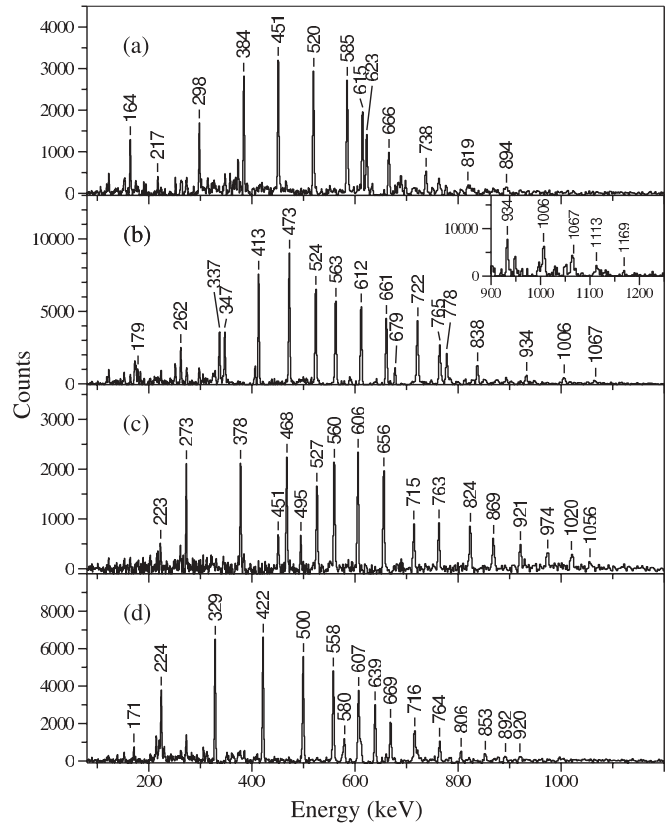

FIG. 8. Representative spectra obtained from triple coincidence gate analysis of (a) the $\alpha = 0$ signature of band 10, (b) the $\alpha = 1$ signature of band 10, (c) the $\alpha = 0$ signature of band 11, and (d) the $\alpha = 1$ signature of band 11.

scenario; however, none were identified at this time owing the lack of intensity near the top of these bands.

B. Band 2: $\pi h_{9/2} \nu i_{13/2}$

The semidecoupled nature of band 2 indicates that both the quasiproton and quasineutron display significant amounts of signature splitting. This leaves only the $\pi h_{9/2}$, $\pi d_{3/2}$, and $\nu i_{13/2}$ orbitals as possible components for its configuration. Since negative parity was determined for band 2, the $\pi h_{9/2} \nu i_{13/2}$ configuration is the most likely candidate. The alignment profile, shown in Fig. 9(b), indicates that the $\alpha = 1$ sequence has a crossing near 0.34 MeV, whereas the $\alpha = 0$ sequence has one near 0.40 MeV. The former crossing is associated with the BC alignment as the slight delay (with respect to the crossings found in the other bands of ^{170}Ta) is characteristic of the $\pi h_{9/2}$ orbital [30]. Thus, the $\alpha = 1$ sequence is assigned as the $G_p A$ configuration, where G_p is the favored ($\alpha = +1/2$) signature of the $\pi h_{9/2}$ orbital. CSM calculations predict that the AD crossing should occur approximately 0.05 MeV higher than the BC one, in good agreement with the alignment seen in the $\alpha = 0$ sequence of band 2. With this AD assignment, the configuration for the $\alpha = 0$ sequence is most likely $G_p B$ and both signatures are associated with $K^\pi = 2^-$. Figure 13(a) provides the comparison of the experimental $B(M1)/B(E2)$ ratios with the theoretical values of the $\pi h_{9/2} \nu i_{13/2}$ configuration, and a good agreement is achieved. Thus, we are in agreement with the assignment proposed by Zhang *et al.* [4] for this structure.

C. Band 3: $\pi h_{9/2} \nu i_{13/2}$

Band 3 strongly feeds into the the $G_p A$ sequence of band 2 through a series of dipole transitions. The alignment profile of band 3, displayed in Fig. 9(b), is nearly identical to the $G_p A$ sequence where a crossing with $\Delta i_x \approx 7\hbar$ is found at 0.34 MeV. This is likely the delayed BC crossing, indicating that the $h_{9/2}$ quasiproton and the $i_{13/2}$ quasineutron are involved in its configuration. Thus, band 3 is assigned the $H_p A$ configuration ($K^\pi = 3^-$), which couples the unfavored signature of the $\pi h_{9/2}$ orbital to the favored $i_{13/2}$ quasineutron. The energy difference seen in Fig. 5(a) is similar to that observed between the signature partners of the $\pi h_{9/2}$ structure in ^{169,171}Ta [15,16], an observation consistent with this assignment.

D. Band 4

Figure 9(b) displays the alignment profile of band 4 and indicates that this structure is likely completing the BC crossing at the lowest observed levels. This suggests that the A quasineutron is involved with its configuration. Following the crossing, band 4 has approximately $1\hbar$ more alignment than the $G_p A$ and $H_p A$ sequences. The $\pi h_{9/2} \nu i_{13/2}$

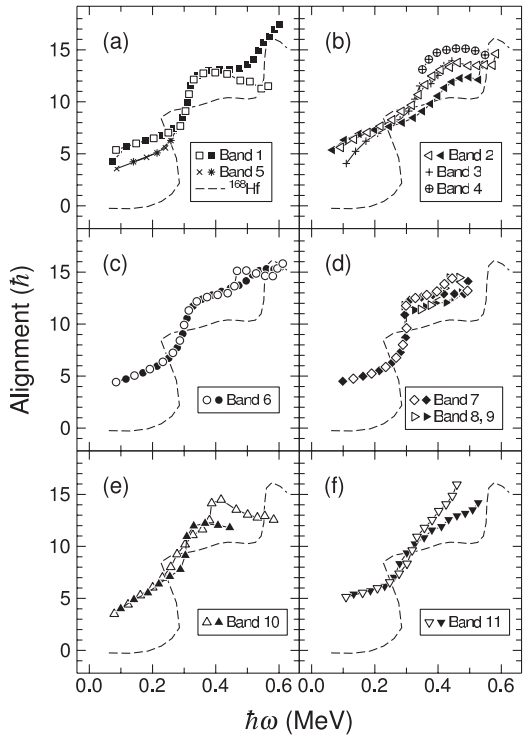

FIG. 9. Alignments for the bands in ^{170}Ta; Harris parameters [24] of $\mathcal{J}_0 = 28\ \hbar^2/\text{MeV}$ and $\mathcal{J}_1 = 58\ \hbar^4/\text{MeV}^3$ were used. The ^{168}Hf yrast band is shown to illustrate the well-known AB neutron crossing ($\hbar\omega \sim 0.27$ MeV) and the E_pF_p proton crossing ($\hbar\omega \sim 0.55$ MeV). Filled (empty) symbols denote the $\alpha = 0$ (1) signature.

configurations should have the largest amount of alignment for two-quasiparticle bands, so it is possible band 4 is initially

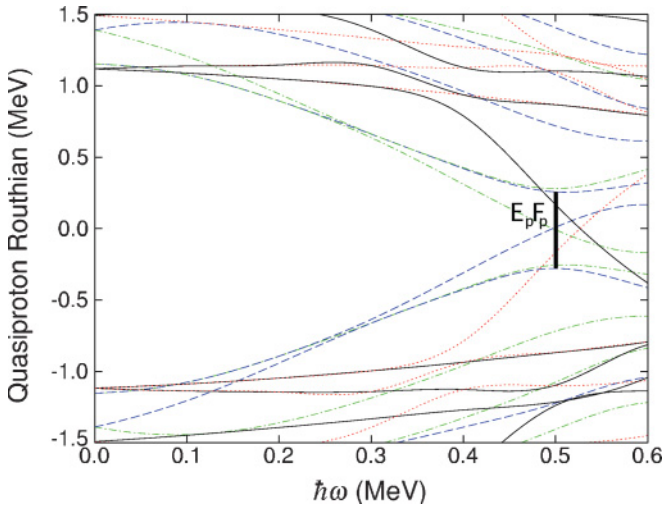

FIG. 10. (Color online) Cranked shell-model calculations for quasiprotons in ^{170}Ta. Deformation parameters $\beta_2 = 0.24$, $\beta_4 = 0$, and $\gamma = 0^\circ$ were used [15,16]. The pairing energy was determined from experimental masses using the five-point fit procedure described in Ref. [26]. The lowest crossing is denoted. Solid lines correspond to configurations having $(\pi, \alpha) = (+, +1/2)$, dotted lines to those having $(+, -1/2)$, dashed-dotted lines to those having $(-, +1/2)$, and dashed lines to those having $(-, -1/2)$.

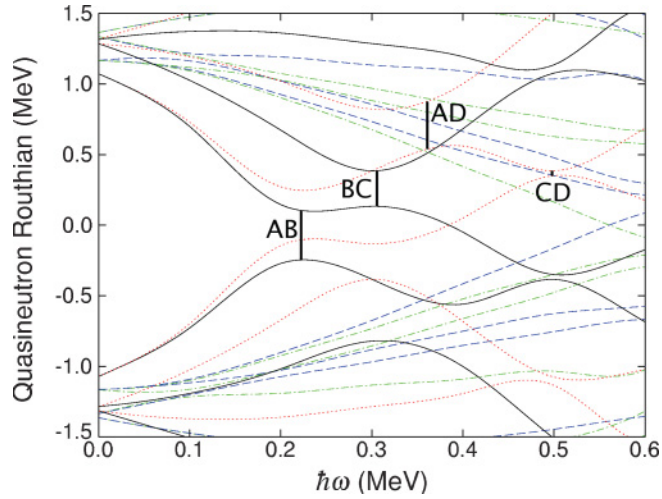

FIG. 11. (Color online) Cranked shell-model calculations for quasineutrons in ^{170}Ta. Deformation parameters $\beta_2 = 0.24$, $\beta_4 = 0$, and $\gamma = 0^\circ$ were used [15,16]. The pairing energy was determined from experimental masses using the five-point fit procedure described in Ref. [26]. The lowest four crossings are denoted. Lines are labeled in the same fashion as described in the previous figure.

based on four quasiparticles. Since this structure is decoupled, it seems likely that all four quasiparticles would be associated with significant signature splitting. The $h_{9/2}$ quasiproton and $i_{13/2}$ quasineutron satisfy these requirements and are likely involved in band 4. It is possible that the $d_{3/2}$ proton is involved as well, but then a positive-parity neutron would be required to achieve an overall negative parity. The $i_{13/2}$ quasineutron is the only positive-parity neutron near the Fermi surface, but if two $i_{13/2}$ quasineutrons were involved, the BC crossing would not be observed. Thus, the configuration of band 4 is not clear at this time. Once again, it should be noted that band 4 may cross with band 1 near $I = 40\hbar$.

E. Band 5: $\pi(h_{11/2}, d_{5/2}, g_{7/2})\nu i_{13/2}$

The fragmented decay of band 5 to both a negative-parity band ($\pi h_{11/2}\nu i_{13/2}$) and a positive-parity sequence

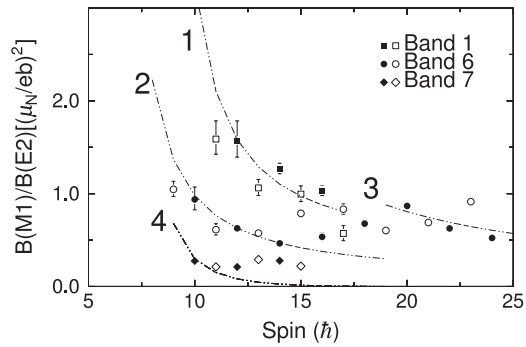

FIG. 12. Measured $B(M1)/B(E2)$ ratios for bands 1, 6, and 7 in ^{170}Ta. Filled (empty) symbols represent the experimental values for the $\alpha = 0$ (1) sequence. Theoretical calculations for bands 1, 6, and 7 are represented as dashed lines with the following configurations: 1: $\pi h_{11/2}\nu i_{13/2}$; 2: $\pi d_{5/2}\nu i_{13/2}$; 3: $\pi d_{5/2}\nu i_{13/2}BC$; 4: $\pi g_{7/2}\nu i_{13/2}$.

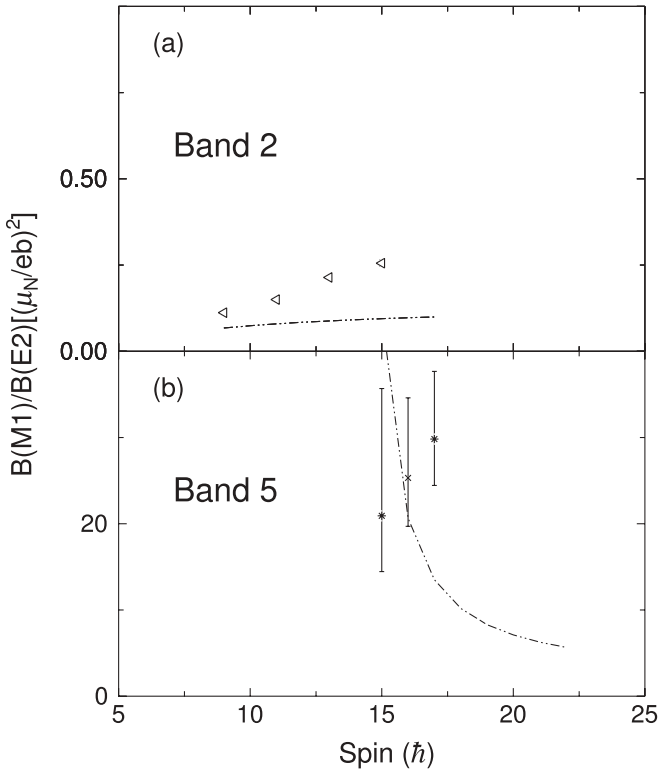

FIG. 13. Measured $B(M1)/B(E2)$ ratios for bands 2 and 5 in ^{170}Ta. Filled (empty) symbols represent the experimental values for the $\alpha = 0$ (1) sequence. (a) The theoretical calculation for band 2 is represented as a dashed line and is interpreted as the $\pi h_{9/2}\nu i_{13/2}$ configuration. (b) The theoretical calculation for band 5 is shown as a dashed line and is the $\pi(h_{11/2},d_{5/2},g_{7/2})\nu i_{13/2}$ configuration.

$(\pi d_{5/2}\nu i_{13/2})$ indicates that it is likely composed of quasiparticles similar to those associated with the latter bands. Four-quasiparticle states are known in the heavier odd-odd tantalum isotopes [31] where they were interpreted as resulting from a coupling between the π^3 ([402]5/2, [404]7/2, [514]9/2) configuration and an $i_{13/2}$ neutron orbital ([633]7/2 in ^{176}Ta and [624]9/2 in ^{178}Ta). Since the neutron Fermi level lies lower in the $i_{13/2}$ shell for ^{170}Ta, the configuration of band 5 is suggested as π^3([402]5/2, [404]7/2, [514]9/2)ν([642]5/2) with $K^\pi = 13^-$. This assignment was also confirmed by comparison of the observed states with results from multi-quasiparticle blocking calculations, similar to those performed for the heavier tantalum nuclei [31]. The proposed $\pi^3\nu^1$ $K^\pi = 13^-$ configuration was calculated to be at an energy near where band 5 was observed. The alignment diagram for band 5 [see Fig. 9(a)] supports this assignment as the band is beginning the BC crossing near 0.3 MeV, indicating the presence of the $i_{13/2}$ quasineutron. Owing to the weakness of the $E2$ transitions, only a few $B(M1)/B(E2)$ ratios could be extracted, as seen in Fig. 13(b). These few ratios are significantly larger than any of the other observed values in the other structures, which also indicates a high-K structure for this band. The theoretical calculation for the proposed configuration agrees well with these few data points; therefore, band 5 is assigned to this $K^\pi = 13^-$ structure.

F. Band 6: $\pi d_{5/2}\nu i_{13/2}$

The strongly coupled nature of band 6 indicates at least one of the quasiparticles responsible for its intrinsic structure must have small signature splitting. In Fig. 9(c), the alignment for band 6 displays a crossing of $\sim 7\hbar$ at $\hbar\omega = 0.30$ MeV, suggesting that the BC alignment is observed in both signatures. Therefore, the A quasineutron is associated with both signatures of band 6, and a quasiproton that would produce little signature splitting must be considered. Protons occupying either the $d_{5/2}$[402]5/2 or $g_{7/2}$[404]7/2 orbitals are possibilities as both are observed at low excitation energies in ^{169,171}Ta [15,16]. The experimentally observed $B(M1)/B(E2)$ ratios are plotted in Fig. 12 along with the theoretical predictions for the $\pi d_{5/2}\nu i_{13/2}$ (line 2) and $\pi g_{7/2}\nu i_{13/2}$ (line 4) configurations. It is evident that the former agrees best with the values for band 6; thus, the A_pA and B_pA configurations ($K^\pi = 5^+$) are assigned to the $\alpha = 1$ and 0 signatures, respectively. This assignment is in agreement with that proposed by Zhang *et al.* [4].

At higher frequencies, the two signatures undergo separate alignments. In the B_pA ($\alpha = 0$) sequence, an alignment of $\sim 1.5\hbar$ is observed at 0.5 MeV. Based upon the CSM calculations of Fig. 10, which displays the lowest proton crossing near 0.5 MeV, we assign this alignment gain to the E_pF_p crossing. A different crossing is observed in the A_pA ($\alpha = 1$) sequence at 0.46 MeV. It is possible that this is a result of the same E_pF_p alignment, but it is not clear why the crossing would occur at different frequencies in the two signatures. Perhaps an unobserved sequence is energetically close to band 6 at this frequency and disturbs the levels to produce the interaction seen in Fig. 9(c).

G. Band 7: $\pi g_{7/2}\nu i_{13/2}$

Similar to band 6, band 7 is strongly coupled in nature and displays the BC crossing at 0.31 MeV in its alignment plot [Fig. 9(d)]. Once again, this indicates the presence of the A quasineutron in both signatures. $B(M1)/B(E2)$ ratios for band 7 are compared in Fig. 12 with the calculated values for the $\pi g_{7/2}\nu i_{13/2}$ configuration. A good agreement is observed, and, therefore we have assigned the C_pA and D_pA configurations to the $\alpha = 1$ and 0 sequences, respectively. Although the G-M rules suggest that $K = 1$ should be favored, the high-K coupling was found to be $\sim$400 keV lower in energy than the low-K coupling of the $\pi g_{7/2}\nu i_{13/2}$ band in ^{164}Tm [10]. In addition, it was found the high-K coupling of band 7 had a better agreement with the predicted additivity of Routhians (see Sec. IV K) than the low-K assignment. Thus, $K^\pi = 6^+$ has been assumed for this sequence. The $\alpha = 0$ sequence remains rather flat following the BC alignment until the highest observed frequency, which may be associated with the onset of the E_pF_p crossing near 0.5 MeV. However, in a similar fashion as in band 6, the $\alpha = 1$ sequence exhibits a crossing at a lower frequency (0.42 MeV) than its signature partner. It seems unlikely that this corresponds to the E_pF_p alignment, and perhaps an unseen band interacts with this signature that causes the alignment gain.

H. Bands 8 and 9

From the rigid-rotor plot of Fig. 5(b), these two sequences are likely to be signature partners. In addition, based on the excitation energy of the bands and the amount of alignment bands 8 and 9 possess [see Fig. 9(d)], these are likely associated with four-quasiparticle structures. Without further information, it is difficult to definitively assign a configuration. However, we tentatively propose the E_pEAB and F_pEAB configurations based on the following arguments. These configurations have positive parity and are composed of orbitals near the Fermi surface. The AB quasineutrons provide $\sim 9\hbar$ of alignment, whereas the E and $E_p(F_p)$ quasiparticles are each associated with approximately $1\hbar$ of alignment. The addition of these alignments sums to $11\hbar$, which agrees well with the initial alignments for bands 8 and 9, as seen in Fig. 9(d). Clearly, further information on bands 8 and 9 is required to confirm or correct these tentative assignments.

I. Band 10: $\pi h_{9/2}\nu h_{9/2}$

Band 10 has the least amount of initial alignment of all the bands with a value close to $3\hbar$, whereas all the other bands have values closer to $5\hbar$. This may indicate that the $i_{13/2}$ quasineutron is not involved in this structure. To obtain $\sim 3\hbar$ of initial alignment, the $h_{9/2}$ quasiproton is likely associated with the band and would need to be coupled with a negative-parity quasineutron to obtain the positive parity associated with the band. The E and F quasineutrons from the $h_{9/2}$ shell are observed in the neighboring ^{169}Hf [21] and ^{171}W [22] nuclei. In the latter it is found that the E signature aligns more rapidly through the AB crossing than the F sequence in a manner very similar to that seen in the odd-spin versus even-spin structures in band 10 [see Fig. 9(e)]. Therefore, band 10 is proposed to be associated with the $\pi h_{9/2}\nu h_{9/2}$ configuration ($K^\pi = 3^+$), where the G_pE and G_pF assignments are given to the $\alpha = 1$ and 0 sequences, respectively. The crossing near 0.3 MeV is associated with the AB alignment, which is delayed from that observed in ^{168}Hf. However, this is consistent with the AB alignments observed in bands involving the $h_{9/2}$ quasiprotons as the slightly larger deformation causes the delay.

At higher frequencies, the $\alpha = 1$ sequence of band 10 experiences an interaction that raises the alignment near 0.4 MeV, but the alignment values then decrease back to the values of its signature partner [Fig. 9(e)]. This is a behavior similar to that seen in the $\alpha = 1$ sequences of bands 6 and 7. It is interesting to note the trend of the frequencies for which this interaction occurs in the three bands: 0.46 MeV in band 6, 0.43 MeV in band 7, and 0.38 MeV in band 10. Each band lies at progressively higher energy and the interactions occur at lower frequency as the excitation energy increases. Perhaps there is a single positive-parity, $\alpha = 1$ structure that interacts with each of these three bands and causes the disturbed alignments at different frequencies. However, further experimental investigation is required to verify this interpretation.

J. Band 11: $\pi d_{3/2}\nu i_{13/2}$

The initial alignment of band 11 ($\sim 5\hbar$) and the observed BC crossing near 0.3 MeV [Fig. 9(f)] are once again consistent with the presence of an $i_{13/2}$ quasineutron. Since the two sequences are decoupled, the quasiproton associated with this band must have a low K value as well and be of positive parity. The only orbital near the Fermi surface that satisfies these requirements is the $d_{3/2}[411]1/2$ state. Indeed, calculated $B(M1)/B(E2)$ ratios for the $\pi d_{3/2}\nu i_{13/2}$ configuration are quite low, 0.1–0.2 $[\mu_N/(e\ \mathrm{b})]^2$, which explains why few intraband $M1$ transitions were observed. Therefore, the I_pA and J_pA configurations ($K^\pi = 2^+$) are assigned to the $\alpha = 1$ and 0 sequences of band 11, respectively. At higher frequencies, the alignments of both signatures continue to increase above the BC crossing. Perhaps, this is the result of the E_pF_p crossing, but this is a dramatically different alignment gain and crossing frequency compared to the assigned E_pF_p crossing in bands 6 ($\pi d_{5/2}\nu i_{13/2}$) and 7 ($\pi g_{7/2}i_{13/2}$). The gain may instead be a result of incorrect Harris parameters, owing to a difference in deformation for band 11 compared to the other bands. Unfortunately, at this point, the nature of the alignment gain near 0.4 MeV for band 11 remains unclear.

K. Additivity of Routhians

To further validate the configuration assignments, a comparison of the experimental Routhians can be made with respect to the sum of Routhians resulting from the one-quasiparticle bands in the neighboring odd-A nuclei [32]. The Routhian for a rotational band is defined as

$$e'(\omega) = E'(\omega) - E'_{\mathrm{ref}}(\omega), \tag{4}$$

where $E'(\omega) = E - \hbar\omega I_x$, $\hbar\omega = dE/dI_x$, and the reference energy in the Harris description [24] is

$$E'_{\mathrm{ref}}(\omega) = -\frac{1}{2}\omega^2\mathcal{J}_0 - \frac{1}{4}\omega^4\mathcal{J}_1 + \frac{1}{8\mathcal{J}_0}. \tag{5}$$

The same Harris parameters used for the alignments were also applied to calculate the Routhians. In addition, the energy of the lowest level observed in band 6 was set to zero.

The present analysis requires the interpolation of the Routhians at a specific rotational frequency ($\hbar\omega = 0.20$ MeV) for the neighboring odd-Z (^{169,171}Ta [15,16]) and odd-N (^{169}Hf [21] and ^{171}W [22]) nuclei. The average summed energy values of the odd-Z and odd-N systems were used to compare

TABLE III. Comparison of measured Routhian values [e' (actual)] of bands in ^{170}Ta with the sum of Routhians from neighboring nuclei. The difference, $\Delta e'$, is equal to the measured Routhian minus the sum of the average Routhians from the neighboring odd-A nuclei, where the Harris parameters $\mathcal{J}_0 = 28\hbar^2/\mathrm{MeV}$ and $\mathcal{J}_1 = 58\hbar^4/\mathrm{MeV}^3$ were used.

Band	Configuration ($\pi\nu$)	K^π	α	e' (actual)	$\Delta e'$ ($\hbar\omega = 0.20$ MeV)
1	E_pA, F_pA	7^-	1,0	−0.87, −0.87	0.03, 0.03
2	G_pA, G_pB	2^-	1,0	−1.19, −1.13	0.19, −0.06
3	H_pA	3^-	0	−0.82	0.05
6	A_pA, B_pA	5^+	1,0	−0.97	−0.01
7	C_pA, D_pA	6^+	1,0	−0.79	0.1
10	G_pE, G_pF	3^+	1,0	−0.83, −0.83	−0.05, −0.05
11	I_pA, J_pA	2^+	1,0	−0.92, −0.96	−0.02, −0.13

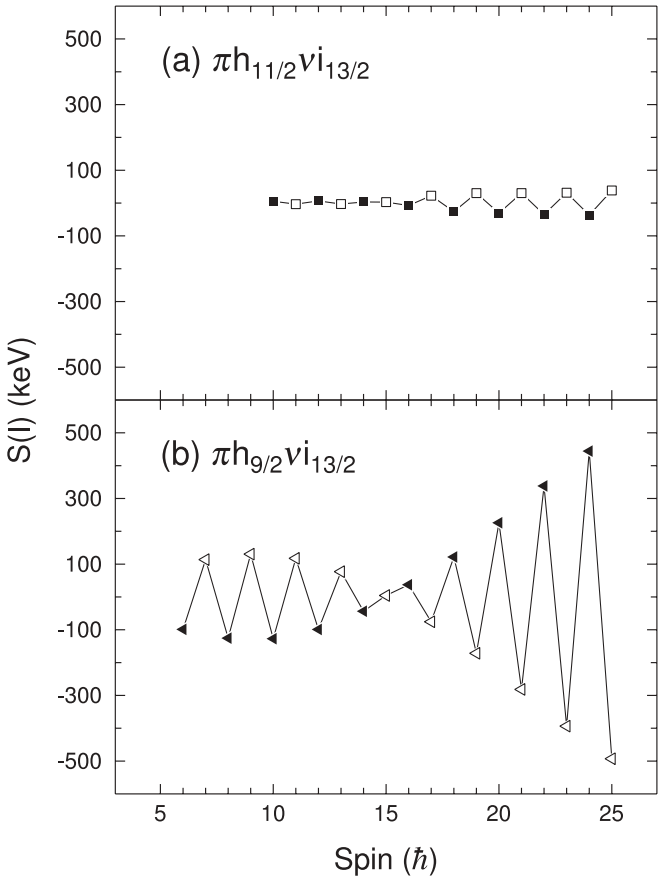

FIG. 14. Signature splitting function, $S(I)$ (as defined in text), vs spin for the (a) $\pi h_{11/2}\nu i_{13/2}$ and (b) $\pi h_{9/2}\nu i_{13/2}$ bands in ^{170}Ta. The $\alpha = 0$ (1) signature is displayed by solid (empty) symbols.

with the observed values in ^{170}Ta. The results from adding the one-quasiparticle Routhians together and comparing them with the corresponding Routhian in odd-odd ^{170}Ta are given in Table III.

The majority of the bands have their Routhians within 50 keV of the summed ones, suggesting that the assigned configurations are correct. These small differences are the result of residual interactions; that is, effects not included in the mean field [32]. As mentioned before, the favored K coupling for band 7 could be discerned based on the additivity of Routhians. If the $K = 1$ coupling is assumed (which is predicted by the G-M rules), $\Delta e' = -0.2$ MeV is found. If $K = 6$ is assumed, $\Delta e'$ is only 0.1 MeV; therefore, the latter coupling is favored. There are two cases where the discrepancy is even larger: G_pA ($\Delta e' = 0.19$ MeV) and J_pA (-0.13 MeV). Similar differences were noted for the G_pA and J_pA configurations in ^{164}Tm [10] and were suggested to be a result of the pn interaction that is responsible for signature inversion, a property discussed next.

V. SIGNATURE INVERSION

The phenomenon of signature inversion, where at low spins the predicted favored signature lies at higher energy than its partner, has been well documented in various regions of the nuclear chart (see Ref. [7] and references therein). In the $A \approx 170$ region, at least two configurations display this effect in odd-odd nuclei: $\pi h_{9/2}\nu i_{13/2}$ and $\pi h_{11/2}\nu i_{13/2}$. The predicted favored signature is simply the sum of the favored signatures of the constituents quasiparticles in the configurations. Therefore, the $\pi h_{9/2}\nu i_{13/2}$ configuration has a favored signature of $\alpha_f = 1$ as $\alpha_f = +1/2$ for both the $h_{9/2}$ quasiproton and the $i_{13/2}$ quasineutron. However, inspection of band 2 in Fig. 1 reveals the $\alpha = 0$ signature is lower in energy at low spin, but the band reverts to the expected ordering at higher spin. This effect is amplified in Fig. 14, which plots the signature splitting function, $S(I) = E(I) - E(I-1) - 1/2[E(I+1) - E(I) + E(I-1) - E(I-2)]$, versus spin for the $\pi h_{11/2}\nu i_{13/2}$ and $\pi h_{9/2}\nu i_{13/2}$ bands in ^{170}Ta. The signature inversion is seen in both bands at lower spin, although the amplitude is clearly much less in the $\pi h_{11/2}\nu i_{13/2}$ sequence than in the $\pi h_{9/2}\nu i_{13/2}$ structure.

Exactly where this reversion occurs is useful for understanding the strength of the forces responsible for creating the inversion. That is, if the reversion takes place at higher spin, it is likely that the inverting force is stronger in that nucleus. Many previous studies that have discussed signature inversion

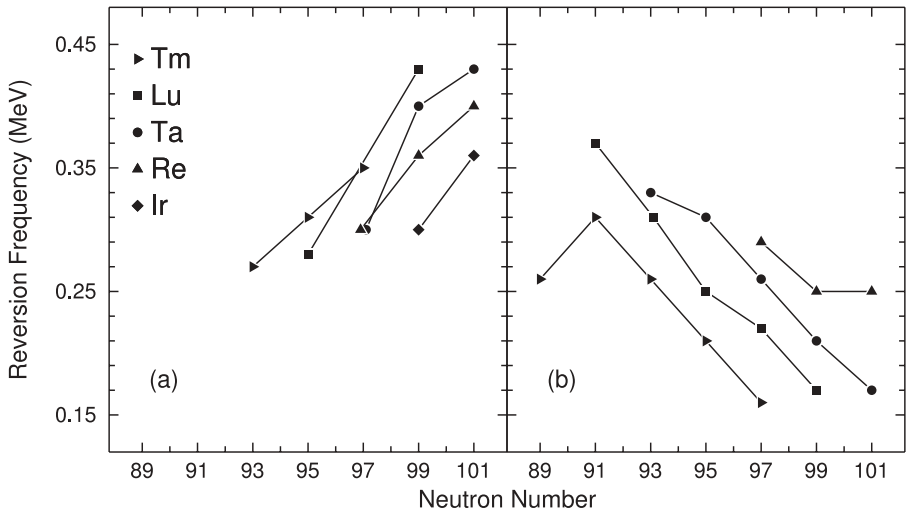

FIG. 15. Reversion frequency, as defined in the text, for the $\pi h_{9/2}\nu i_{13/2}$ (left panel) and the $\pi h_{11/2}\nu i_{13/2}$ bands (right panel) in the $A \approx 170$ region.

focus on the spin at which the reversion occurs, but since these are all odd-odd nuclei, spin is not well established in the majority of the nuclei considered. It is perhaps more useful to consider the reversion frequency, which is the frequency where the Routhians of the signatures cross [7,33]. As discussed in Ref. [33], this frequency is nearly independent in a range of a few $\hbar$ of possible spin assignments.

The reversion frequencies of the $\pi h_{9/2}\nu i_{13/2}$ and $\pi h_{11/2}\nu i_{13/2}$ bands are displayed in Figs. 15(a) and 15(b), respectively. Opposing trends are clearly visible in these plots:

(i) For a given neutron number, the reversion frequency decreases with Z for the $\pi h_{9/2}\nu i_{13/2}$ configuration, whereas it increases in the $\pi h_{11/2}\nu i_{13/2}$ bands.
(ii) For a given element, the reversion frequency increases with N for the $\pi h_{9/2}\nu i_{13/2}$ configuration, whereas it decreases for the $\pi h_{11/2}\nu i_{13/2}$ one.

These trends can be explained rather naturally when applying the general rules established in Ref. [10] where signature inversion was investigated with the particle-rotor model including a *pn* interaction. Reviol *et al.* determined that the *pn* interaction drives the band toward signature inversion if either the proton or neutron is more particle-like (i.e., the particle is below the $\Omega = 1/2$ orbital of its shell) and the other is more hole-like (the orbital lies above the low-Ω orbitals of its shell). For example, in ^{164}Tm, the proton $h_{9/2}$ orbital is one MeV above the Fermi surface, whereas the neutron is just above the $\Omega = 5/2$ orbital of the $i_{13/2}$ shell and the *pn* interaction was found to be the root cause of the observed inversion. However, if both proton and neutron act as particles or both as holes, the *pn* interaction does not support inversion.

The decrease of the reversion frequency with Z for the $\pi h_{9/2}\nu i_{13/2}$ band, trend (i), can naturally be explained with this model. As Z increases, the Fermi surface moves closer to and into the $\pi h_{9/2}$ shell. Thus, it evolves from particle-like to hole-like. The neutron remains hole-like for a given N, so one would indeed expect the *pn* interaction to be strongest for the lower Z isotopes and create a higher reversion frequency, as observed. The opposite is occurring in the $\pi h_{11/2}\nu i_{13/2}$ band where the proton is becoming more hole-like as Z increases and the Fermi surface is near the top of the shell. Therefore, the higher Z nuclei should exhibit the highest reversion frequency for a given N, as is indeed seen in Fig. 15(b).

The general trend of decreasing reversion frequencies with N for a given isotopic chain for the $\pi h_{11/2}\nu i_{13/2}$ band, trend (ii), is also accounted for. As N increases in the $i_{13/2}$ shell, there is a greater mixture of hole and particle states in the wave function, which weakens the *pn* force supporting the inversion. Only ^{158}Tm ($N = 89$) does not follow this trend, but there is likely a large deformation change between $N = 91$ and 89 that is responsible for this anomaly. Finally, the increasing reversion frequency with N for the $\pi h_{9/2}\nu i_{13/2}$ bands can be explained when the deformation trend is also considered. As N increases toward midshell ($N = 104$), the deformation increases; therefore, the orbitals in the $h_{9/2}$ proton shell are energetically farther apart. This will make the proton more purely associated with the $\Omega = 1/2$ component and, thus, more particle-like. Therefore, inversion will be supported more robustly even as the increasing neutron Fermi surface results in a greater admixture of particle-hole components as it approaches $N = 104$.

VI. SUMMARY

A comprehensive spectroscopic study of the odd-odd nucleus ^{170}Ta has been performed and eleven rotational structures have now been identified. The relative excitation energies of these bands are at present all known, which is a rare feature when compared with other odd-odd isotopes. Configurations were proposed for most of the structures where bands were based on every quasiproton observed in ^{169,171}Ta, except for the $\pi i_{13/2}$ one. The additivity of Routhians confirmed the configuration assignments except in a few cases. One of those cases was in the $\pi h_{9/2}\nu i_{13/2}$ structure, which is also known for its signature inversion at low spins. Indeed, by using the particle-hole coupling scheme with a *pn* interaction, as outlined in Ref. [10], the differing trends in this configuration, as well as in the $\pi h_{11/2}\nu i_{13/2}$ bands of the $A \approx 170$ region, could be understood.

ACKNOWLEDGMENTS

The authors thank the ANL operations staff at Gammasphere and gratefully acknowledge the efforts of J. P. Greene for target preparation. We also thank D. C. Radford for his software support. This work is funded by the National Science Foundation under Grant Nos. PHY-0456463 (FSU) and PHY-0554762 (USNA), as well as by the US Department of Energy, Office of Nuclear Physics, under Contract Nos. DE-AC02-06CH11257 (ANL), DE-FG02-94ER40848 (UML), and DE-FG02-96ER40983 (UT).

[1] A. J. Kreiner, Phys. Rev. C **38**, R2486 (1988).
[2] K. Starosta *et al.*, Phys. Rev. Lett. **86**, 971 (2001).
[3] R. Bengtsson, H. Frisk, F. R. May, and J. A. Pinston, Nucl. Phys. A **415**, 189 (1984).
[4] Y. H. Zhang *et al.*, Phys. Rev. C **60**, 044311 (1999).
[5] F. Meissner, W.-D. Schmidt-Ott, V. Freystein, T. Hild, E. Runte, H. Salewski, and R. Michaelsen, Z. Phys. A **337**, 45 (1990).
[6] Y. Liu, Y. Ma, H. Yang, and S. Zhou, Phys. Rev. C **52**, 2514 (1995).
[7] G. García Bermúdez and M. A. Cardona, Phys. Rev. C **64**, 034311 (2001).
[8] Z.-C. Gao, Y. S. Chen, and Y. Sun, Phys. Lett. B **634**, 195 (2006).
[9] A. K. Jain and A. Goel, Phys. Lett. B **277**, 233 (1992).
[10] W. Reviol *et al.*, Phys. Rev. C **59**, 1351 (1999).
[11] M. Matsuzaki, Phys. Lett. B **269**, 23 (1991).
[12] N. Tajima, Nucl. Phys. A **572**, 365 (1994).
[13] R. V. F. Janssens and F. S. Stephans, Nucl. Phys. News **6**, 9 (1996).

[14] D. C. Radford, Nucl. Instrum. Methods Phys. Res. A **361**, 297 (1995).
[15] D. J. Hartley *et al.*, Phys. Rev. C **72**, 064325 (2005).
[16] D. J. Hartley *et al.*, Phys. Rev. C **74**, 054314 (2006).
[17] M. Cromaz *et al.*, Nucl. Instrum. Methods Phys. Res. A **462**, 519 (2001).
[18] K. Starosta *et al.*, Nucl. Instrum. Methods Phys. Res. A **515**, 771 (2003).
[19] R. E. Leber, P. E. Haustein, and I.-M. Ladenbauer-Bellis, J. Inorg. Nucl. Chem. **38**, 951 (1976).
[20] J. C. Bacelar *et al.*, Nucl. Phys. A **442**, 547 (1985).
[21] K. A. Schmidt *et al.*, Eur. Phys. J. A **12**, 15 (2001).
[22] J. Espino *et al.*, Nucl. Phys. A **567**, 377 (1994).
[23] R. Bengtsson and S. Frauendorf, Nucl. Phys. A **327**, 139 (1979).
[24] S. M. Harris, Phys. Rev. **138**, B509 (1965).
[25] R. B. Yadav *et al.*, Phys. Rev. C **80**, 064306 (2009).
[26] P. Möller and J. R. Nix, Nucl. Phys. A **536**, 20 (1992).
[27] A. Bohr and B. Mottelson, *Nuclear Structure* (Benjamin, New York, 1975), Vol. 2.
[28] F. Dönau, Nucl. Phys. A **471**, 469 (1987).
[29] C. J. Gallagher and S. A. Moszkowski, Phys. Rev. **111**, 1282 (1958).
[30] H. J. Jensen *et al.*, Nucl. Phys. A **695**, 3 (2001).
[31] F. G. Kondev *et al.*, Nucl. Phys. A **632**, 473 (1998).
[32] S. Frauendorf *et al.*, Nucl. Phys. A **431**, 511 (1984).
[33] D. J. Hartley *et al.*, Phys. Rev. C **65**, 044329 (2002).